

Depositional facies and stratal cyclicity of dolomites in the Lower Qiulitag Group (Upper Cambrian) in northwestern Tarim Basin, NW China

Yanqiu Zhang · Daizhao Chen · Xiqiang Zhou ·
Zenghui Guo · Wenwen Wei · Maria Mutti

Received: 21 May 2014 / Accepted: 12 September 2014 / Published online: 19 November 2014
© Springer-Verlag Berlin Heidelberg 2014

Abstract The Upper Cambrian Lower Qiulitag Group in the Tarim Basin, NW China, is overwhelmingly composed of cyclic dolomites. Based on extensive field investigations and facies analysis from four outcrop sections in the Bachu-Keping area, northwestern Tarim Basin, four main types of facies are recognized: open-marine subtidal, restricted shallow subtidal, intertidal, and supratidal facies, and these are further subdivided into ten lithofacies. In general, these facies are vertically arranged into shallowing-upward, metre-scale cycles. These cycles are commonly composed of a thin basal horizon reflecting abrupt deepening, and a thicker upper succession showing gradual shallowing upwards. Based on the vertical facies arrangements and changes across boundary surfaces, two types of cycle: peritidal and shallow subtidal cycle, are further identified. The peritidal cycles, predominating over the lower-middle Lower Qiulitag Group, commence with shallow subtidal to lower intertidal facies and are capped by inter-supratidal facies. In contrast, the shallow subtidal cycles, dominating the upper Lower Qiulitag Group, are capped by shallow-subtidal facies. Based on vertical lithofacies variations, cycle stacking patterns,

and accommodation variations revealed by Fischer plots, six larger-scale third-order depositional sequences (Sq1–Sq6) are recognized. These sequences generally consist of a lower transgressive and an upper regressive systems tract. The transgressive tracts are dominated by thicker-than-average cycles, indicating an overall accommodation increase, whereas the regressive tracts are characterized by thinner-than-average peritidal cycles, indicating an overall accommodation decrease. The sequence boundaries are characterized by transitional zones of stacked thinner-than-average cycles, rather than by a single surface. These sequences can further be grouped into lower-order sequence sets: the lower and upper sequence sets. The lower sequence set, including Sq1–Sq3, is characterized by peritidal facies-dominated sequences and a progressive decrease in accommodation space, indicating a longer-term fall in sea level. In contrast, the upper sequence set (Sq4–Sq6) is characterized by subtidal facies-dominated sequences and a progressive increase in accommodation space, indicating a longer-term rise in sea level.

Keywords Dolomites · Facies · Stratal cyclicity · Sequences · Upper Cambrian · Tarim Basin · China

Electronic supplementary material The online version of this article (doi:10.1007/s10347-014-0417-1) contains supplementary material, which is available to authorized users.

Y. Zhang · D. Chen (✉) · X. Zhou · Z. Guo · W. Wei
Key Laboratory of Petroleum Resources Research, Institute
of Geology and Geophysics, Chinese Academy of Sciences,
Beijing 100029, China
e-mail: dzh-chen@mail.iggcas.ac.cn

Y. Zhang · M. Mutti
Institute of Earth and Environmental Science, University
of Potsdam, Karl-Liebknecht-Str. 24–25, 14476 Potsdam-Golm,
Germany

Introduction

High-frequency metre-scale cycles are basic building units of shallow-water carbonate successions and they are commonly organized into larger-scale depositional sequences. Many thick shallow-water carbonate successions are characterized by a clear hierarchical stratal cyclicity which is widely considered to having been driven by variable-order sea-level fluctuations (Fischer

1964; Goldhammer et al. 1990, 1993; Fischer and Botjer 1991; Montañez and Osleger 1993; Mutti and Simo 1993; Strasser and Hillgartner 1998; Strasser et al. 2000; Chen et al. 2001; Hofmann et al. 2004; Hofmann and Keller 2006; Laya et al. 2013). Such stratal cyclicity in platform carbonates can be shown by the vertical cycle stacking patterns, which are commonly illustrated by use of the Fischer plot (Fischer 1964; Goldhammer et al. 1987; Read and Goldhammer 1988; Osleger and Read 1993; Chen et al. 2001; Chen and Tucker 2003). Many studies have documented the cycles and/or sequences of Upper Cambrian shallow-water carbonate successions, such as those in North China (Meng et al. 1997; Shi et al. 1997; Mei et al. 2005), and North America (Chow and James 1987; Koerschner and Read 1989; Read 1989; Hardie et al. 1991; Osleger 1991a; Osleger and Read 1991; Glumac and Walker 2000).

The Tarim Basin is the largest petroliferous basin in China where a number of oil and gas fields have been discovered in the last two decades, with production taking place from Lower Paleozoic strata, particularly Ordovician carbonates (Li et al. 1996; Zheng et al. 2007; Lin et al. 2011). More recently, there has been an increasing interest in more deeply buried (generally >5 km) Cambrian dolomites. Thus it is imperative to investigate the facies types and their tempo-spatial variations in a time-defined (cycle and sequence) stratigraphic framework; this in turn will facilitate a better understanding of deposition and platform evolution, and prediction of favorable dolomite reservoirs and their distribution. Although some studies have recognized the larger-scale depositional sequences of the Cambrian dolomites in the Tarim Basin (Chen et al. 2006; Fan et al. 2007; Zhao et al. 2010; Yang and Liu 2011), few studies have been carried out on the high-frequency, metre-scale cycles. This has resulted in many uncertainties in the identification of the larger-scale depositional sequences of the platform carbonates and in our understanding of platform evolution.

This study aims (1) to describe the lithofacies and metre-scale cycles in the Lower Qiulitag Group of the Upper Cambrian in the NW Tarim Basin, with a view to deducing the depositional environments, (2) to illustrate the vertical cycle stacking patterns and hierarchy of stratal cyclicity using the graphic tool of Fischer plots; and (3) to determine the third-order sequences in the Lower Qiulitag Group and their correlation with those in the coeval carbonate successions elsewhere around the world. This study could refine the time-stratigraphic framework for the Upper Cambrian, which is generally devoid of sufficient biostratigraphic controls in the Tarim Basin, and improve our understanding of allogenic forcing of the stratal cyclicity of the enormously thick carbonate successions and platform evolution.

Geological setting

The Tarim Basin, located in the southern part of the Xinjiang Autonomous Region in northwest China, is a cratonic basin bordered by the Tianshan Mountains to the north, the Kunlun Mountains to the southwest and the Albyn Mountains to the southeast (Fig. 1).

Most of the basin was filled with the Precambrian to Permian marine sedimentary strata and Mesozoic-Cenozoic non-marine successions (Li et al. 1996; Jia and Wei 2002). Along the ENE-trending Bachu-Keping-Askui Uplift in the northwest flank of the basin, the Precambrian to Permian rocks, however, were subject to extensive uplift and subsequent exhumation due to collision of the Tarim plate and Tianshan island arc to the north from the Mesozoic onwards (Zhang and Gao 1992; Kang and Kang 1996; Zhou 2001; Jia et al. 2004). In this region, the Cambrian and Ordovician systems are dominated by marine carbonate rocks; the Cambrian succession is overwhelmingly composed of dolomite except for bedded chert and phosphatic black shale in the lowermost Cambrian Yurtus Formation. The Upper Cambrian Lower Qiulitag Group is characterized by thick cyclic dolomites. Within this stratigraphic unit, important age-constrained fossils such as conodonts *Teridontus nakamurai*, *T. reclinatus*, *T. erectus* and the trilobite *Saukiidae* are present (Fig. 2; Zhou et al. 1991; Zhou 2001). The Lower Qiulitag Group is overlain by the Lower Ordovician Penglaiba Formation. A light-colored limestone interval containing Ordovician conodonts *Monocostodus severiensis* and *Teridontus gracilis* occurs commonly in the base of this formation (Supplementary Fig. S1; Zhou et al. 1991; Zhang and Gao 1992), although this marker bed was locally dolomitized as well. The stratigraphic systems and nomenclatures of the Cambrian are shown in Fig. 2 in which the Lower Qiulitag Group of the Upper Cambrian (Furongian) is the focus of this study. The Lower Qiulitag Group consists exclusively of dolomite dominated by microbialite (thrombolite, stromatolite) in the lower portion and microbial boundstone and oolite in the upper part.

Materials and methods

Four sections encompassing the Lower Qiulitag Group were measured and logged bed by bed at Penglaiba (PLB) in Aksu city, Tonggusibulong (TGL) and Keping (KP) in Keping County, and Yong'anba (YAB) in Bachu County, in the western Tarim Basin (Figs. 1, S1). Of these, the PLB section (location: 40°55'12.51"N, 79°53'56.62"E), 297 m thick, is continuously exposed and so is the most complete one. The TGL section, 761 m thick, is well exposed in the Keping area. YAB (64 m thick) and KP (96 m thick) sections, however, only cover the upper part of the Lower Qiulitag Group (Fig. S2).

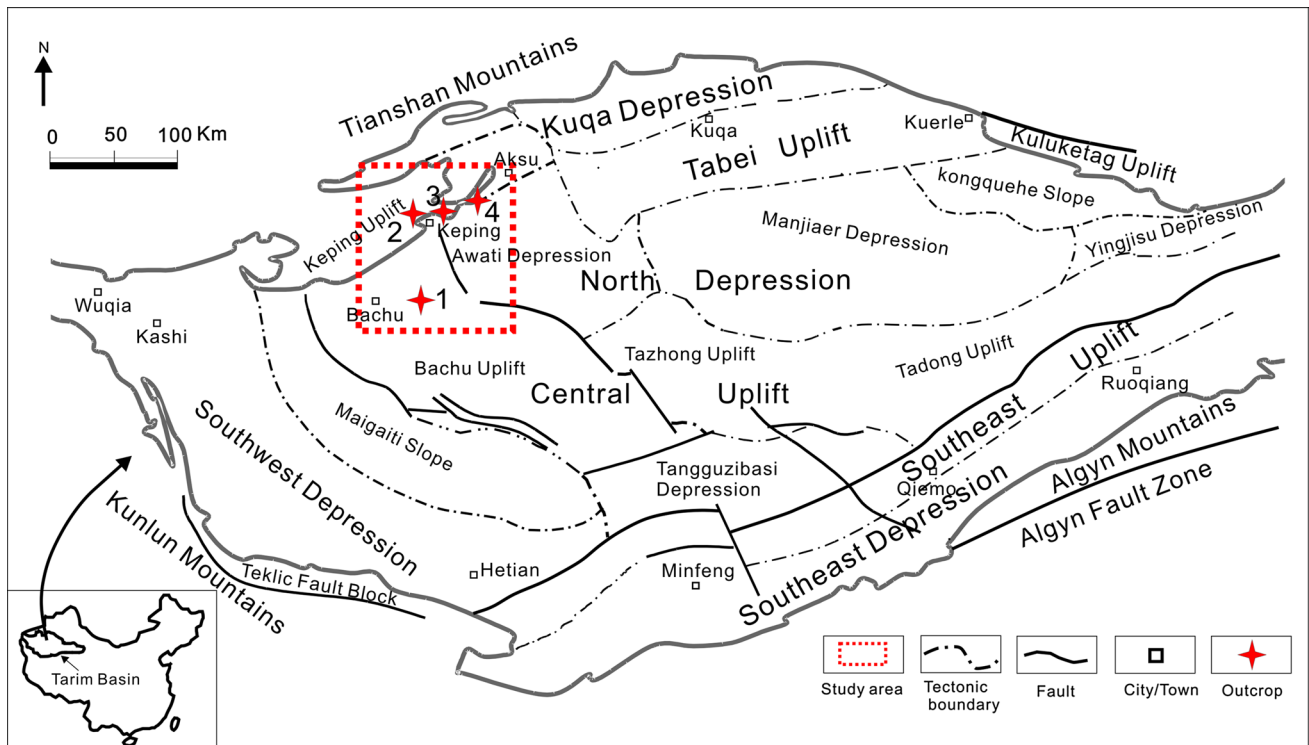
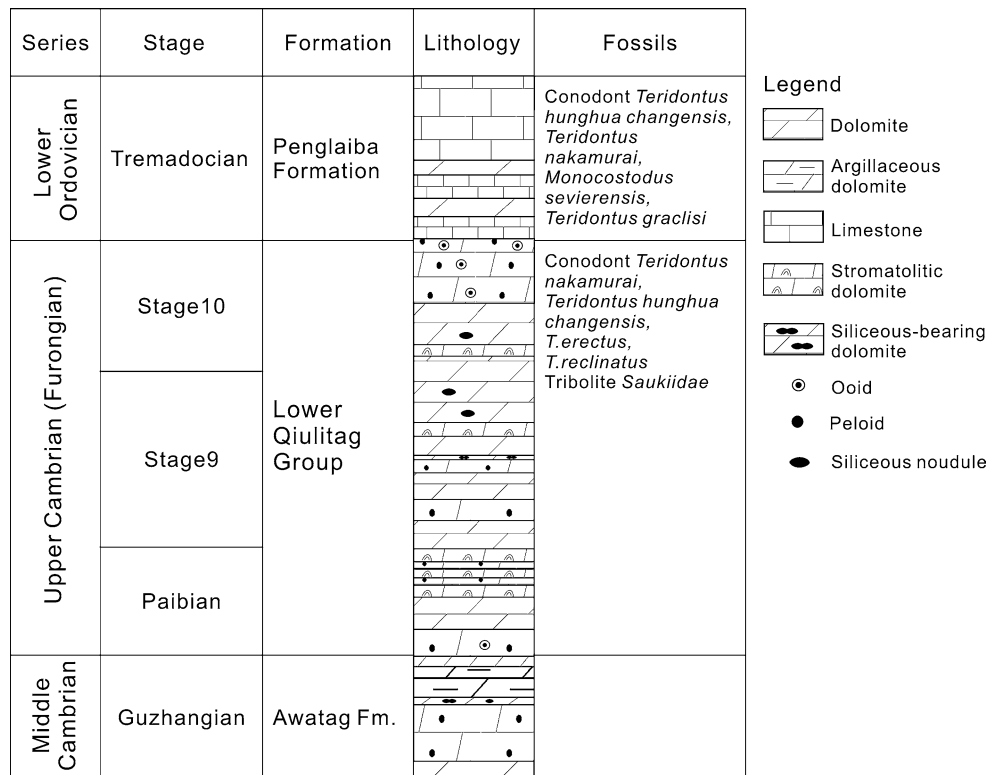


Fig. 1 Location of the study area and general structural units in the Tarim Basin [modified from Lin et al. (2011)]. 1 Yong'anba section (YAB); 2 Keping section (KP); 3 Tonggusibulong section (TGL); 4 Penglaiba section (PLB)

Fig. 2 Cambrian system in the northwestern Tarim Basin, mainly based on data from (Zhou et al. 1990, 1991; Zhang and Gao 1992; Zhou 2001)



The lithofacies of the Lower Qiulitag Group were described and interpreted in terms of lithology, textures/fabrics, sedimentary structures, bed geometry, and color. Hundreds of standard thin-sections from hand samples were prepared for petrographic studies. The terminology employed in description, in principle, follows the carbonate classification of Dunham (1962).

Depositional facies (or environments) were identified and interpreted based on the tempo-spatial relationship and similarity of the lithofacies association described with regard to well-proven diagnostic sedimentary characteristics. High-frequency, metre-scale cycles were identified mainly based on the recurrences of vertically stacked lithofacies (or facies) and their transitional (gradual or abrupt) patterns across the bounding surfaces.

Fischer plots were applied to illustrate vertical cycle stacking patterns and long-term changes in accommodation space on carbonate platforms (Fischer 1964; Sadler et al. 1993; Bosence et al. 2009). Statistical tests using z-scores were applied to determine the degree of randomness and to assist in the interpretation of the origin of these cycles (Sadler et al. 1993; Lehrmann and Goldhammer 1999; Tucker and Garland 2010). Larger-scale third-order sequences were determined based on the cycle stacking patterns and accommodation changes revealed by the Fischer plots, together with facies stacking patterns (i.e., percentage of peritidal facies in each cycle) and depositional indicators.

Depositional facies

Ten lithofacies (L1–L10) were identified in the Lower Qiulitag Group. These lithofacies can be further categorized into several facies associations, representing various depositional environments, such as supratidal, intertidal, restricted subtidal, and open-marine subtidal (Table 1).

Intertidal to supratidal facies

This facies mainly includes the following lithofacies: thin laminite (L1; Fig. 3a, b), thick laminite (L2; Fig. 4a), wavy laminite (L3; Fig. 4b), and stromatolite (L4; Fig. 4c, d), and these predominate over the lower-middle part of the Lower Qiulitag Group. Detailed descriptions can be found in Table 1. Typically, these lithofacies stack vertically into a metre-scale conformable succession from L4 to L1, although incomplete successions comprising parts of these lithofacies are more common (Fig. 5b).

The presence of subaerial exposure features (i.e., mudcracks, reddening) in L1 (Table 1; Fig. 3a) suggests that

it was deposited on a supratidal flat subject to subaerial exposure and rare flooding, probably through large spring tidal and storm currents (Fig. 5b). In this case, the shrinkage flakes or clasts may have been broken into edgewise pebbles (Fig. 3a). Well-rounded quartz silts in the reddened laminites (Fig. 3b, c) were likely transported by wind onto the supratidal flat under an arid climate (Shinn 1983). This scenario also reconciles its stratal occurrence at the top of a vertical conformable lithofacies succession (Fig. 5b).

Facies L2 commonly occurs below L1, and the intercalations of microbial layers and local presence of mudcracks (Table 1; Fig. 4a) indicate deposition on a low-energy tidal flat slightly seawards where microbial mats were developed; occasionally the mats may have been broken up during spring tides and/or storms (Shinn 1983; Tucker et al. 1990; Wright and Burchette 1996).

The widespread presence of microbial components in the wavy laminae of L3 (Table 1; Fig. 4b) indicates deposition in low-energy microbial mats on the intertidal to lower supratidal zone of a tidal flat (Fig. 5b), as has been described from many modern and ancient tidal-flat environments (Shinn 1983; Hardie and Shinn 1986; Chen and Tucker 2003).

The dominance of domical or laterally linked hemispherical (LLH) microbialites in L4 (Table 1; Fig. 4c) with well-developed microbial and/or cryptomicrobial laminae (Fig. 4d), along with its stratigraphic position commonly below L1 to L3 in a vertical conformable succession, indicates that this lithofacies was deposited in an intertidal to restricted shallow subtidal setting (Fig. 5b; Aitken 1967; Ginsburg 1975; Demicco 1983; Pratt et al. 1992; Sherman et al. 2001).

Restricted shallow subtidal to low intertidal facies

Restricted shallow-subtidal to low intertidal facies include stratiform thrombolite (L5; Fig. 6a–d), cross-bedded grainstone lenticle (L6; Fig. 6e) and thin-bedded ribbon (wavy) dolomite (L7; Fig. 6f). Detailed descriptions can be found in Table 1. These lithofacies mainly occur in the lower-middle part of the Lower Qiulitag Group. Vertically, L5 is commonly overlain by L4 (Fig. 4c) and/or L3 in a vertical conformable succession, rarely alternating with them (Figs. 5b, 6c). In a few cases, L6 is intercalated within L5 (Fig. 6e). In some cases, it is underlain by L7 which generally shows wavy and ribbon-like stratification (Fig. 6f).

The dark, irregular to dendroid clotted or spongy fabrics (or mesoclots) in L5 (Table 1; Fig. 6a, b) have been extensively documented and interpreted to be of microbial origin (Aitken 1967; Kennard and James 1986; Shapiro 2000). Microbial filaments present in L5 (Table 1; Fig. 6d) are

Table 1 Summary of lithofacies types in dolomite rocks of the Lower Quliitag Group in NW Tarim Basin

Facies association	Lithofacies/Thickness	Lithology	Description	Biota	Interpretation
Intertidal to supratidal					
	Thin laminite (L1) (0.1–0.6 m)	Alternating Ms with peloidal Ws/Ps, minor well-sorted and rounded quartz silts disseminated	Light grey to grey, yellowish to reddish locally. Thin- to medium-bedded; mm-scale laminae, parallel lamination, flake pebbles intercalated locally, mudcracks common, reddening coloration locally where lamination obscured	Absent	Less agitated upper intertidal to supratidal flats
	Thick laminite (L2) (0.1–1.5 m)	Alternating Ms with peloidal Ps/Ws or microbialite	Light grey to dark grey, reddish locally. Thin- to thick-bedded; cm-scale parallel to subparallel laminae, microbial fabrics intercalated locally, intraclastic pebbles, rare mudcracks and silica bands/nodules	Microbial or cryptomicrobial elements common	Low-energy upper intertidal to supratidal flats
	Wavy laminite (L3) (0.1–2 m)	Alternating peloidal Ws/Ps with microbialites or intergrown microbialites	Grey to dark grey. Thin- to thick-bedded; mm- to cm-scale, mild undulatory laminae; domical stromatolites intercalated locally; minor siliceous nodules	Microbes and/or cryptomicrobes dominant	Low-energy intertidal to the lower supratidal flats
	Stromatolite (L4) (0.1–2 m)	Intergrown microbialites and/or cryptomicrobialites	Grey to dark grey common. Medium- to thick-bedded; laterally linked domical and/or hemispheroidal morphologies (15–60 cm high) dominant, rare discrete columnar forms; smooth to convoluted microbial laminae (1–5 mm thick); siliceous nodules common; fenestral or irregular pores filled by later cements common	Microbes and/or cryptomicrobes exclusively	Restricted shallowest subtidal to intertidal setting
Restricted shallow subtidal to deep intertidal					
	Stratiform thrombolite (L5) (0.2–2.2 m)	Thrombolitic microbialites or Bs	Grey to dark grey. Medium- to massively bedded, stratiform to mild hummocky configuration; mottled appearance (macrofabrics), irregular to dendroid clotted fabrics (mesoclots), complex internal microbial microfabrics (lobate, cellular, grumous, peloidal and micritic), minor microbial filaments remained; abundant fenestrae and irregular pores filled by later cements; fabric obscured common by postdepositional dolomitization and crystallization	Microbes and/or cryptomicrobes dominant	Restricted shallow subtidal to deep intertidal

Table 1 continued

Facies association	Lithofacies/Thickness	Lithology	Description	Biota	Interpretation
	Cross-bedded Gs lentic (L6) (0.2–0.5 m)	Pebbly peloidal/microbial Gs	Grey to dark grey. Thin- to medium-bedded; lens-shaped beds intercalated in thrombolites; erosive bases with lag flat pebbles common; cross-bedded	Microbial fragments	Intertidal creek on microbial mat or tidal washover
	Thin-bedded ribbon (wavy) dolomite (L7) (0.1–0.6 m)	Peloidal Ms to Ps	Grey to dark grey. Thin-bedded; ribbon-like or wavy stratification with wavy to ripple cross-lamination; rare siliceous nodules	Rare skeletal elements (i.e., ostracods)	Restricted shallow subtidal environment
Open-marine subtidal	Oolite (L8) (0.3–6.5 m)	Peloidal-oidial Gs and pebbly (or intraclastic) ooidal Gs common with a few skeletal grains	Light grey to dark grey. Medium- to thick-bedded even massively bedded; well-sorted and grain-supported fabrics; cross-bedding (herringbone bedding) common, discontinuous wavy bedding; basal and internal erosive surfaces common with lag pebbles; structures and grain fabrics obscured commonly by postdepositional dolomitization and crystallization	Trilobites and brachiopods	High-energy shallow subtidal sandy shoals and/or tidal channels
	Microbial buildups (L9) (1–10 m)	Microbial or thrombolitic Bs/Fs	Grey to dark grey. Thick-bedded to massively bedded; discrete columnar morphologies (up to a few metres high) characterized by thrombolitic-like fabrics (or mesoclots), mounded forms (<10 m high) with dendroid to digitate in situ growth structure/fabric, minor microbial filaments preserved; co-occurrence with peloidal-oidial Gs (L8); silicification common	Microbes and/or cryptomicrobes dominant, <i>Girvanella</i> , <i>Renalcis</i> and <i>Epiphyton</i> locally; rare skeletal fossils	Microbial buildups colonizing on subtidal sandy shoals or tidal channels
	Lenticular to platy dolomite (L10) (0.1–1 m)	Peloidal Ws/Ps with minor ooids and a few skeletal grains, minor argillaceous matter	Grey to dark grey. Thin- to medium-bedded; lenticular to platy stratification with more or less argillaceous strips	Trilobites, crinoids and brachiopods	Relatively deep (intermediate) subtidal environment

Ms-dolomudstone, Ws-dolowackestone, Ps-dolopackstone, Gs-dolograinstone, Bs-doloboundstone, Fs-doloframestone

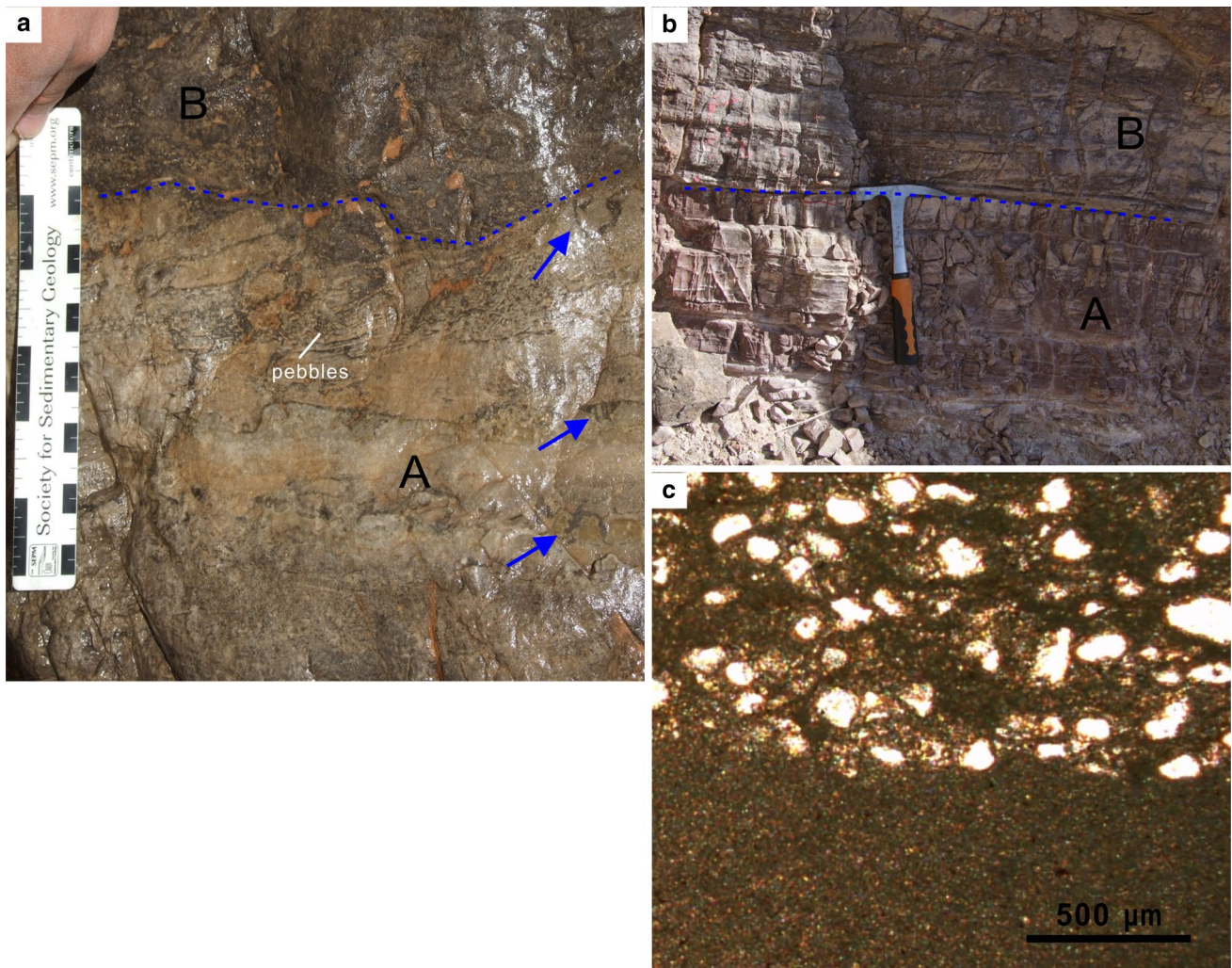


Fig. 3 Supratidal facies in the Lower Qiulitag Group at studied sections. **a** Yellowish grey thin laminite (L1) characterized by alternating millimetre-scale laminae (A) in which mudcracks (blue arrows) and intraformational pebbles are present, and unconformably overlain by the thrombolite (B), TGL section. **b** Purplish vague thin laminite (L1,

A) grades into thickened laminite (L2, B) at PLB section. Hammer for scale (30 cm long). **c** Photomicrograph of purplish thin laminite of (b). Silt-size quartz grains (white color) concentrated within the mudstone. Planar-polarized light

commonly attributed to in situ calcification of coccoid or coccoid-dominated microbial communities (Kennard and James 1986). The vertical stacking relationship with L4 and L3/L2, as noted above, suggests that L5 was formed in a relatively restricted shallow subtidal to low intertidal environment (Aitken 1967). Similar thrombolitic microbialites were also widely reported in the Upper Cambrian (Furongian) Chaomidian Formation in North China (Lee et al. 2010) and in coeval deposits elsewhere where they were also interpreted as having been deposited in restricted shallow subtidal to low intertidal environments (Koerschner and Read 1989; Osleger and Read 1991; Glumac and Walker 2000; Read and Repetski 2012).

The presence of microbial fragments, cross-bedding and grain-supported fabrics in L6 and their occurrence as lensoid intercalations within L5 (Table 1; Fig. 6e) indicate that

L6 was deposited under relatively high-energy conditions, such as within a tidal creek, surrounded by low-energy microbial mats on an intertidal flat (Fig. 5b).

Similar to the ribbon carbonates documented by other researchers (Demico 1983), the presence of wavy and ribbon-like stratification and cross-laminated ripples in L7 and its occurrence commonly beneath microbialites (L4 or L5) in a vertical conformable succession (Table 1; Fig. 6f) indicate that L7 was deposited in deeper water in a relatively restricted, shallow subtidal environment (lagoon) close to microbial mats landwards (Fig. 5b).

Open-marine subtidal facies

This facies mainly includes thick- to massively bedded oolite (L8; Fig. 7), microbial buildup (L9; Fig. 8a, b) and

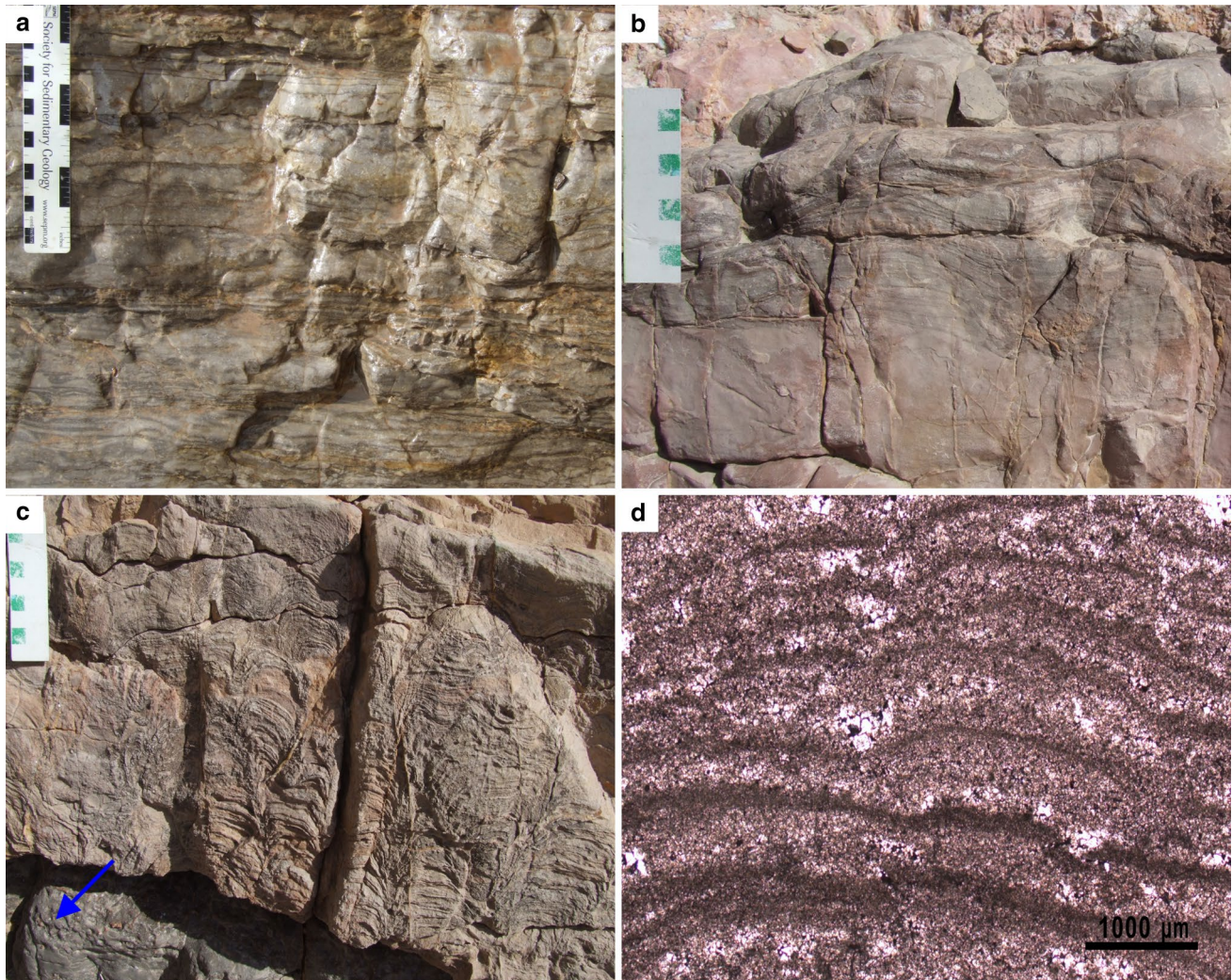


Fig. 4 Intertidal facies. **a** Thick laminite (L2) exhibits with centimetre-scale laminae, TGL section. **b** Wavy laminite (L3) with undulatory laminae, PLB section. *Scale* in centimetres. **c** Columnar (*lower*) to domical (*upper*) stromatolite showing *smooth* to convoluted individual laminae (L4), which overlies the thrombolite (*arrow*), PLB

section. *Scale* in centimetres. **d** Photomicrograph showing microscopic fabrics of stromatolite laminae consisting of repetitive alternations of *dark* cryptmicrobial and *light*-colored, porous micropeloidal couplets, PLB section. Planar-polarized light

lenticular to platy dolomite (L10; Fig. 8c, d). Detailed descriptions are given in Table 1. These lithofacies mainly occur in the mid-upper part of the Lower Qiulitag Group. In this facies, L8, which is rarely overlain by intertidal to supratidal facies (L1 to L3), commonly overlies, but locally co-occurs laterally with L9; in places it is underlain by L10 within vertical metre-scale conformable successions (Fig. 5b).

The dominance of ooids, commonly well sorted with a grain-supported fabric (Table 1; Fig. 7a, b) in L8 point to high-energy wave-agitated conditions within the subtidal high-energy zone (Cloyd et al. 1990; Demicco and Hardie 1994). The presence of basal and internal erosive surfaces, bidirectional cross-bedding, large flat pebbles (or intraclasts) (Table 1; Fig. 7c, d) and large skeletal fragments

(Fig. 7d) on erosive surfaces in some oolites suggest more intense wave erosion downwards into underlying sediments followed by bidirectional current agitation; this may indicate deposition in a tidal channel (Fig. 5b). This lithofacies thus is interpreted to have been deposited mainly on subtidal ooidal shoals, which could have been cut by tidal channels, and prograded into a deeper subtidal environment (i.e., L9 or L10); in some cases the facies aggraded into a shallower intertidal and even supratidal flat (e.g., L1–L3; Fig. 5b).

Similar to L5 as documented above, the presence of internal clotted fabrics (or mesoclots) in L9 (Table 1; Fig. 8a) points to a microbial origin (Aitken 1967; Kennard and James 1986; Shapiro 2000; Riding 2000). However, the isolated columnar morphologies and co-existence with

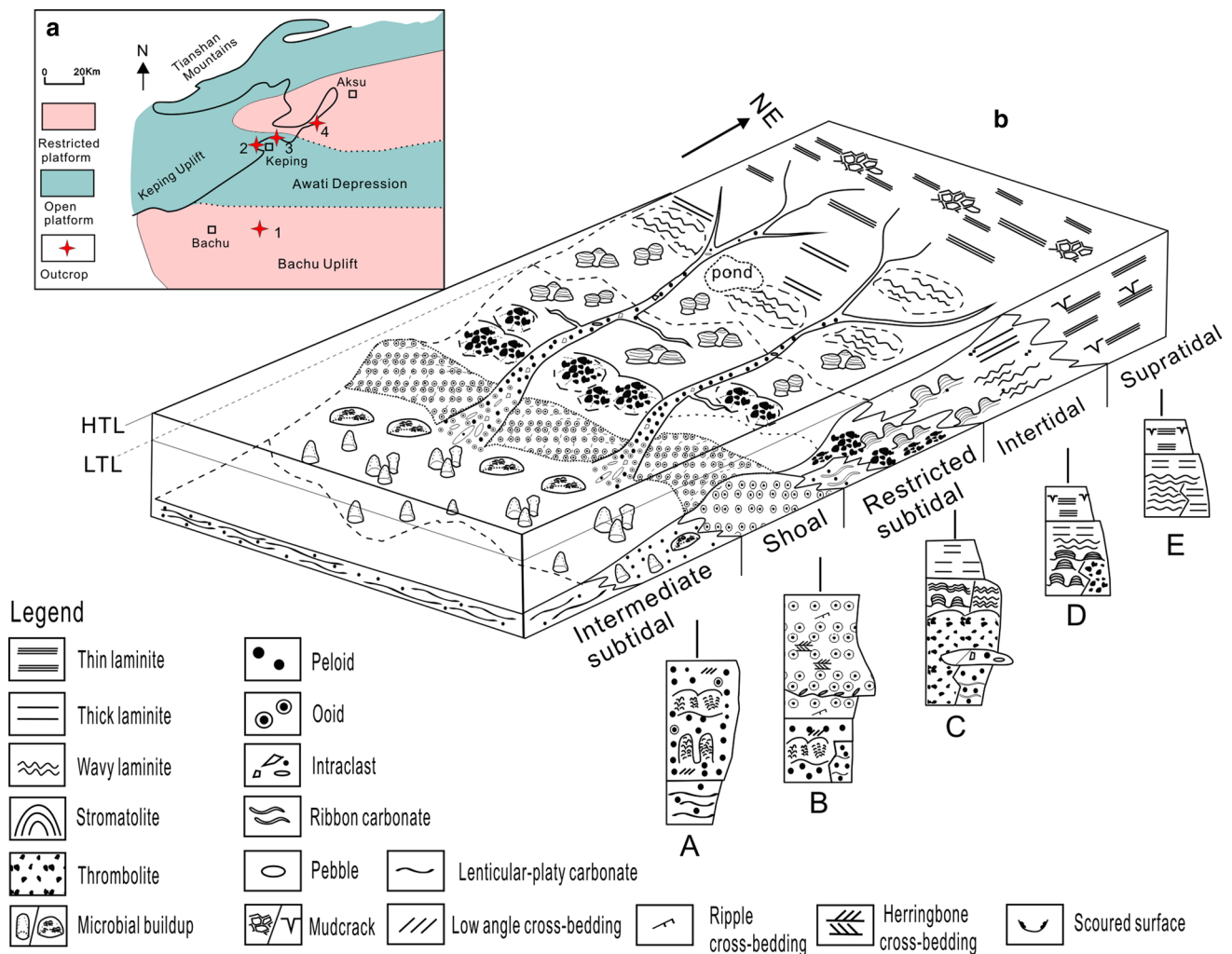


Fig. 5 **a** Paleogeographic map of the Lower Qiulitag Group in the study area. **b** Schematic facies model of a carbonate ramp system in the study area. Note the metre-scale depositional successions (or

cycles, A–E) in different environments, from supratidal, to intertidal, to restricted shallow subtidal, and to shoals and intermediate subtidal facies. *LTL* low tidal level, *HTL* high tidal level

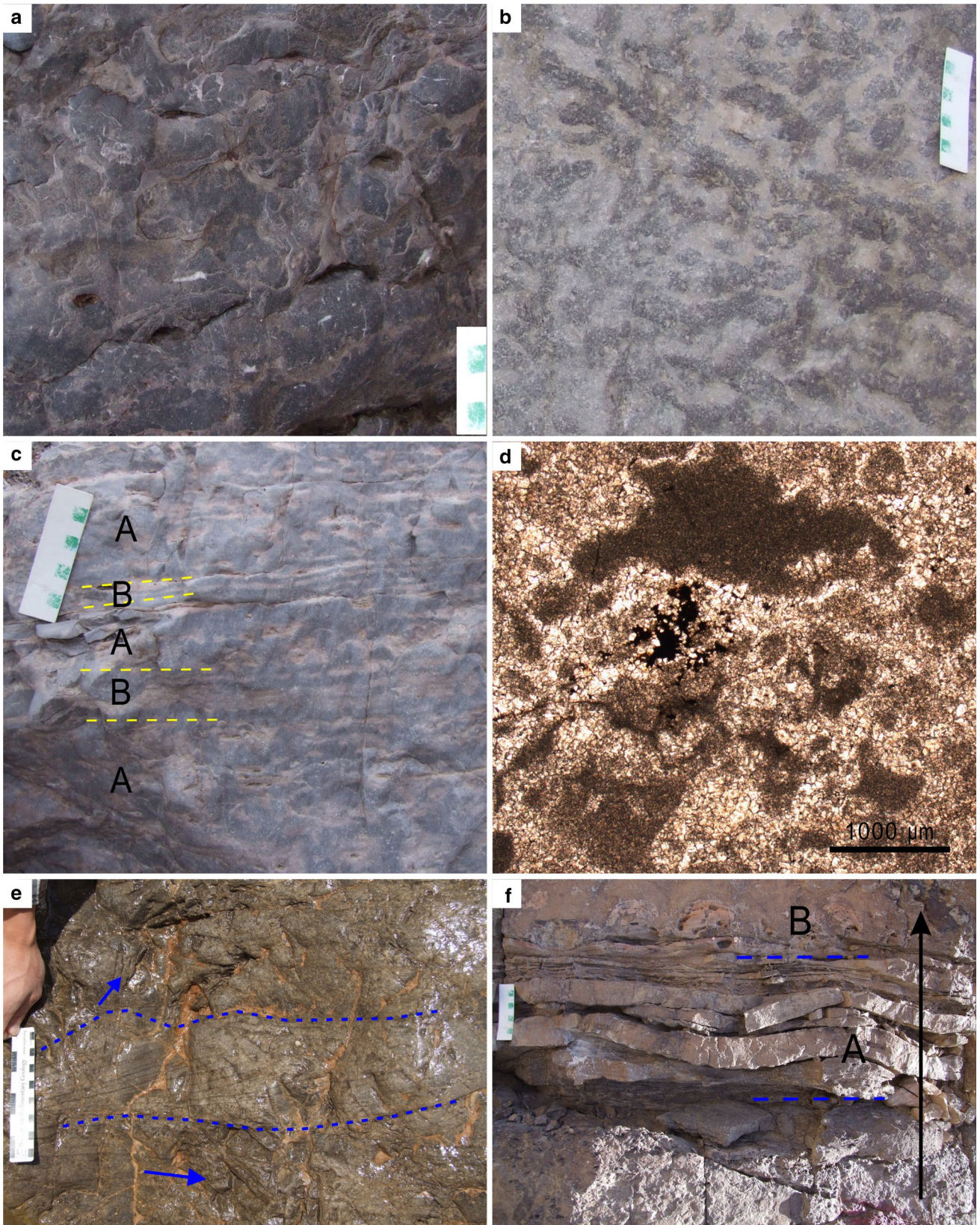
L8 (Fig. 8a) indicate that they are microbial builds (or bioherms) which colonized high-energy wave-influenced subtidal sandy shoals or tidal channels (Aitken 1967; Kennard and James 1986; Wright and Burchette 1996; Feldmann and McKenzie 1998). These builds are similar to those in the Conococheague Formation (Upper Cambrian) of western Maryland (Demico 1985), the Hellnmaria Member of Cordilleran in western United States, and the Copper Ridge Dolomite of southwestern Virginia and Conococheague Formation of northern Virginia, Appalachian (Osleger and Read 1991), where they were interpreted as having been formed on high-energy shoals and in tidal channels as well (Fig. 5b). The dendroid to digitate in situ growth structures (or dendrolites; Riding 2000; Table 1; Fig. 8b) in some microbial mounds (up to tens of metres high) likely reflect a more wave-resistant framework; this is consistent with the high percentage of framework-building

calcimicrobes such as *Girvanella*, *Renalcis* and *Epiphyton* (Table 1).

With facies L10, its lower stratal position commonly overlain by L8 and L9 (Fig. 5b), development of platy to lenticular stratification with wavy to parallel lamination, and a relatively high argillaceous content (Table 1; Fig. 8c) point to deposition in a relatively deep subtidal, open-marine environment (Fig. 5b). This scenario agrees with the presence of a few open-marine skeletal fragments of trilobite and crinoid (Fig. 8d).

High-frequency metre-scale cycles

The Lower Qiulitag Group (Furongian) is characterized by repeated shallowing-upward, metre-scale cycles, ranging from 0.3 to 18 m (average 2.3 m) in thickness. Based



◀ **Fig. 6** Restricted shallow subtidal facies. **a** Mesostructure of stratiform thrombolites (L5) shown by *dark bush-like (lower) to irregular (upper)* mesoclots, PLB section. *Scale in centimetres.* **b** Mesostructure of stratiform thrombolites (L5) displayed by dendroid to digitate mesoclots, PLB section. *Scale in centimetres.* **c** Thrombolites (L5, A) are intercalated with thick laminite (L2, B), PLB section. *Scale in centimetres.* **d** Microstructure of the stratiform thrombolite (L5) with *darker irregular microbial micrite clots (or thrombo-*ses), PLB section. Planar-polarized light. **e** Cross-bedded peloidal/microbial grainstone (L6) intercalation between thrombolites (*arrows*), TGL section. **f** Thin-bedded wavy (or *ribbon*) peloidal wackestones/packstones (L7, A) overlain by stromatolite (B), PLB section. *Scale in centimetres*

on the intracycle facies arrangement and features of the bounding surfaces, two dominant types of cycle are distinguished: peritidal and shallow subtidal. The peritidal cycles

are capped by peritidal facies (Figs. 9, 10a), and these are dominant in the lower-middle part of the Lower Qiulitag Group. In contrast, shallow subtidal cycles are capped by shallow subtidal facies (Fig. 10b), and mainly occur in the upper part of the studied successions.

Peritidal cycles

Based on facies changes across the bounding surfaces, asymmetrical and symmetrical metre-scale cycles are further identified. The asymmetrical cycles, which are dominant, are characterized by a facies jump across the cycle boundaries (Figs. 9, 10a). By contrast, the less common symmetrical cycles exhibit gradual facies changes across the boundaries (Figs. 3b, 9; Elrick 1995; Chen et al. 2001; Tucker and Garland 2010).

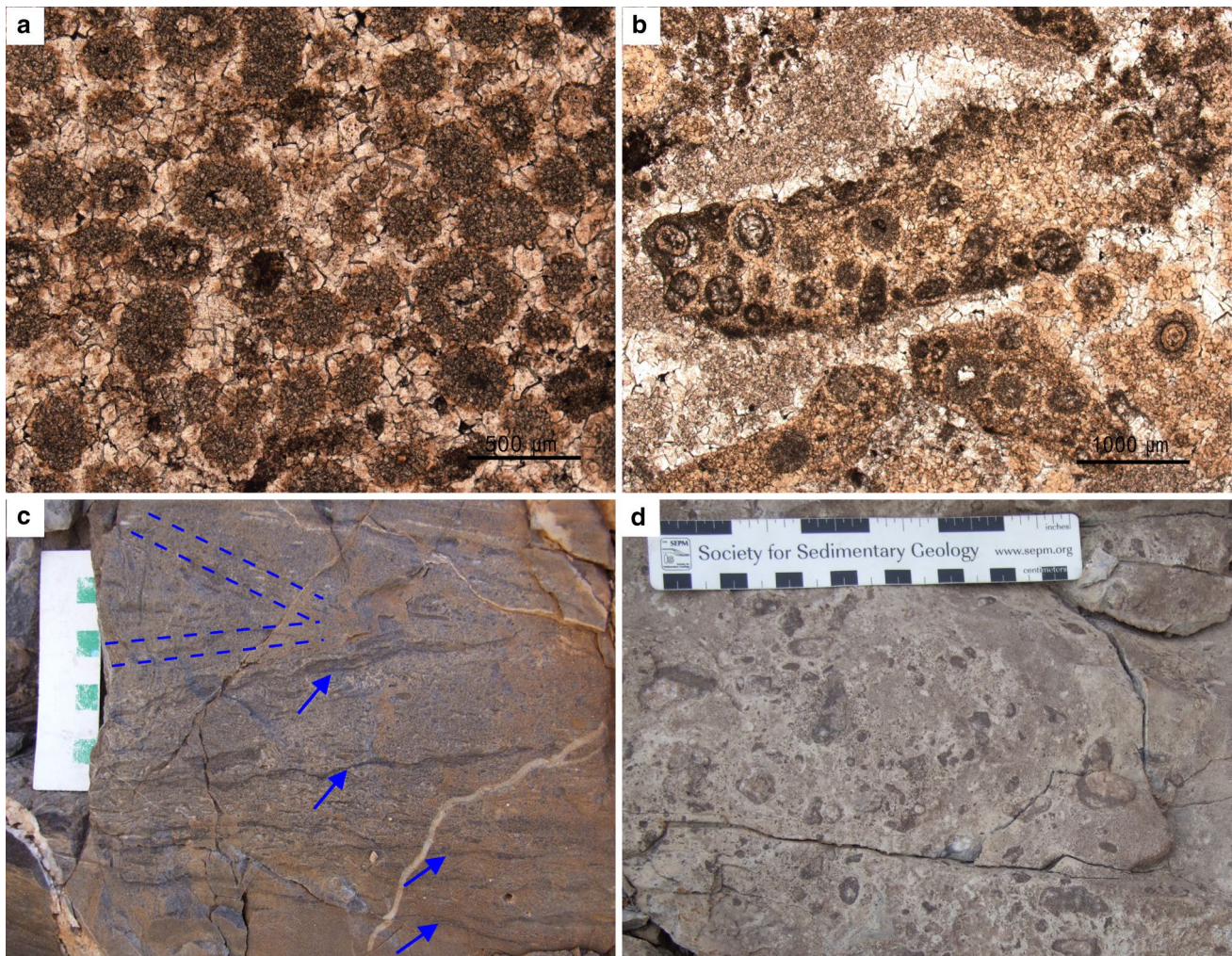


Fig. 7 Shallow subtidal facies. **a** Ooidal grainstone (L8). Note the vague internal fabrics of ooids because of dolomitization and recrystallization, TGL section. Planar-polarized light. **b** Intraclastic peloidal-ooidal grainstone. Note the ooids and peloids within the intraclasts, indicating multiple erosive processes, KP section. Planar-

polarized light. **c** Cross-bedded (*dashed lines*), pebbly peloidal-ooidal grainstone (L8) with multiple internal erosion surfaces (*arrows*), KP section. *Scale in centimetres.* **d** Bioclastic peloidal-ooidal grainstone (L8) with skeletal pebbles, TGL section

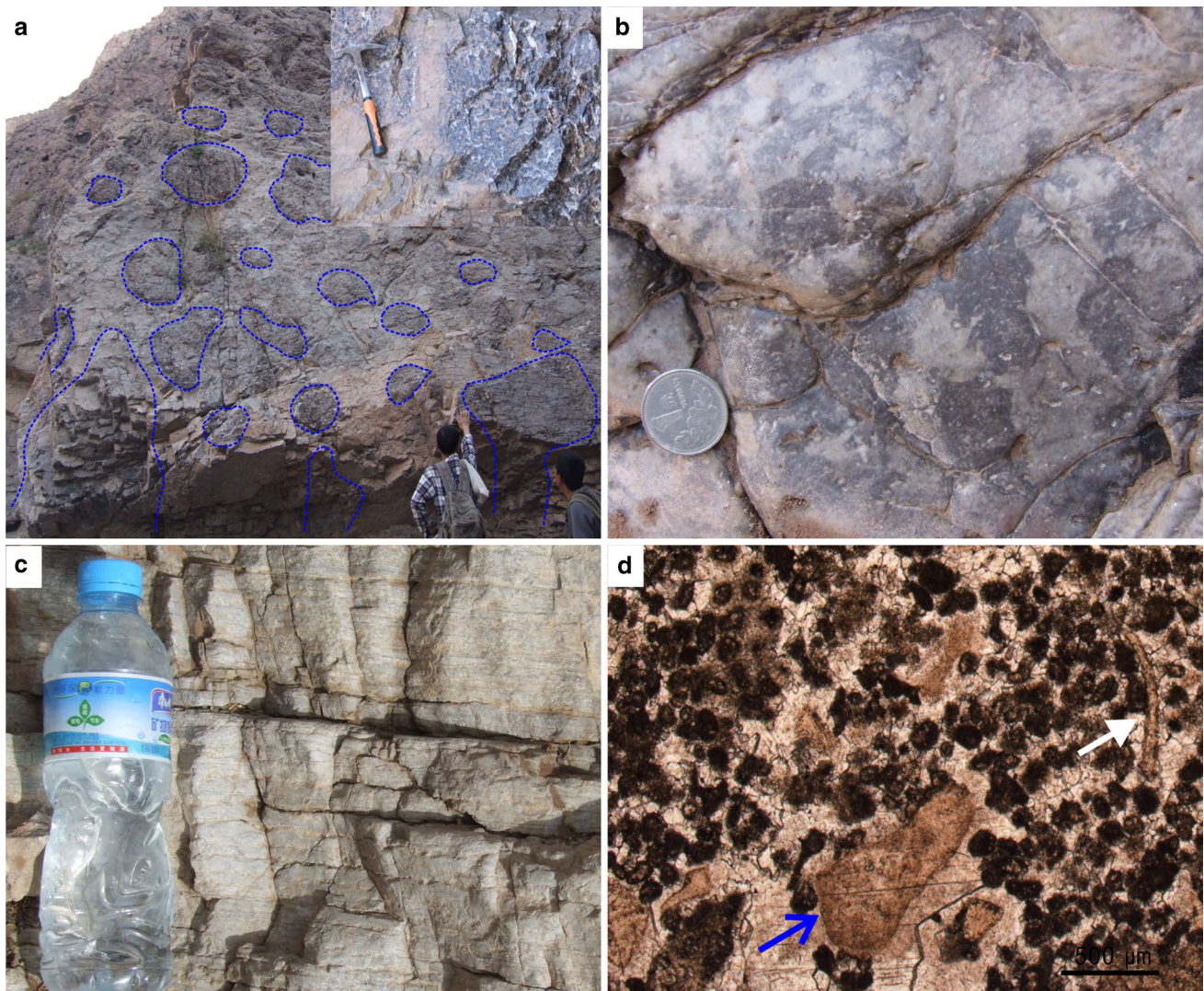


Fig. 8 Subtidal facies. **a** A view of the mostly isolated, columnar microbial (thrombolite) buildups (L9, *circled*) which could have been laterally linked when growing upwards. Interhead areas were filled with peloidal-oidal grainstones (*light-colored*), upper part of Qiu-litag Group, TGL section. Standing person (*left*) for scale (~0.7 m). Inset photo shows the internal fabrics of the microbialite (*Hammer* is 30 cm); **b** In situ palmate-lobate and bushy growth fabrics of

microbial framestone (L9) with infills of peloidal-oidal grainstones (*light-colored*) in the framework cavities, TGL section. *Coin* for scale (2.5 cm across). **c** Thin-bedded platy to lenticular peloidal wackestones to grainstones (L10) with thin argillaceous partings, TGL section. *Bottle* for scale (22 cm). **d** Photomicrograph of lithofacies L10 of (c). Note the crinoid (*blue arrow*) and trilobite (*white arrow*) fragments. Planar-polarized light

The asymmetrical metre-scale cycles are interpreted to reflect a rapid deepening above the boundaries followed by a prolonged shallowing process. They are typical of 'regressive-prone' successions (Elrick 1995). The basal facies of these cycles can comprise a variety of facies, from subtidal to intertidal facies, including lithofacies L5–L2, depending on the depositional site on the tidal flat (Fig. 5b). These basal facies may be overlain by prograding, shallower upper intertidal to supratidal facies (lithofacies L3–L1), forming repeated asymmetrical, shallowing-upward cycles. Of these, the thrombolite-based peritidal cycle is the most common (Fig. 10a), and comprises basal

L5 facies, typically followed by L4 through L1 upwards, although L6 may be intercalated locally as a result of truncation by the migration of relatively high-energy tidal channels (or creeks) across the inter-supratidal flat (Figs. 5b, 6e).

In contrast, the symmetrical cycles start with laminites (L3 or L2) akin to those in the tops of underlying cycles but they are commonly darker in color and do not exhibit subaerial exposure features (Figs. 5b–E, 9); these represent a gradual facies transition between the two bounding cycles. The thin transgressive basal facies are then succeeded by prolonged regressive successions, the same as those seen

Fig. 9 Vertical lithofacies successions within the typical peritidal cycles in the Lower Qiulitag Group, PLB section. The lower cycle is composed of basal ribbon dolomite (L7), thrombolite (L5), stromatolite (L4), wavy laminite (L3) and thin laminite (L1), in ascending order. The upper cycle, a symmetrical one, in ascending order, comprises thick laminite (L2), wavy laminite (L3) and thin laminite (L1). *Hammer* for scale (30 cm long). See the lithological logs on the *right* for details

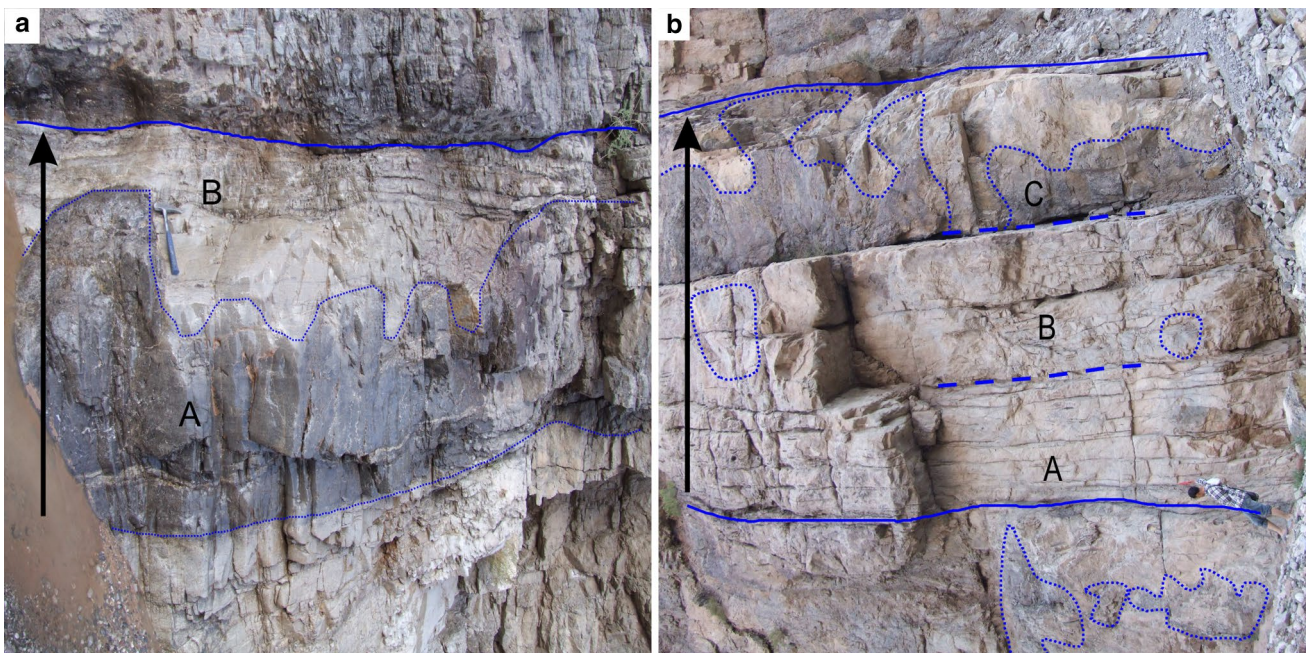
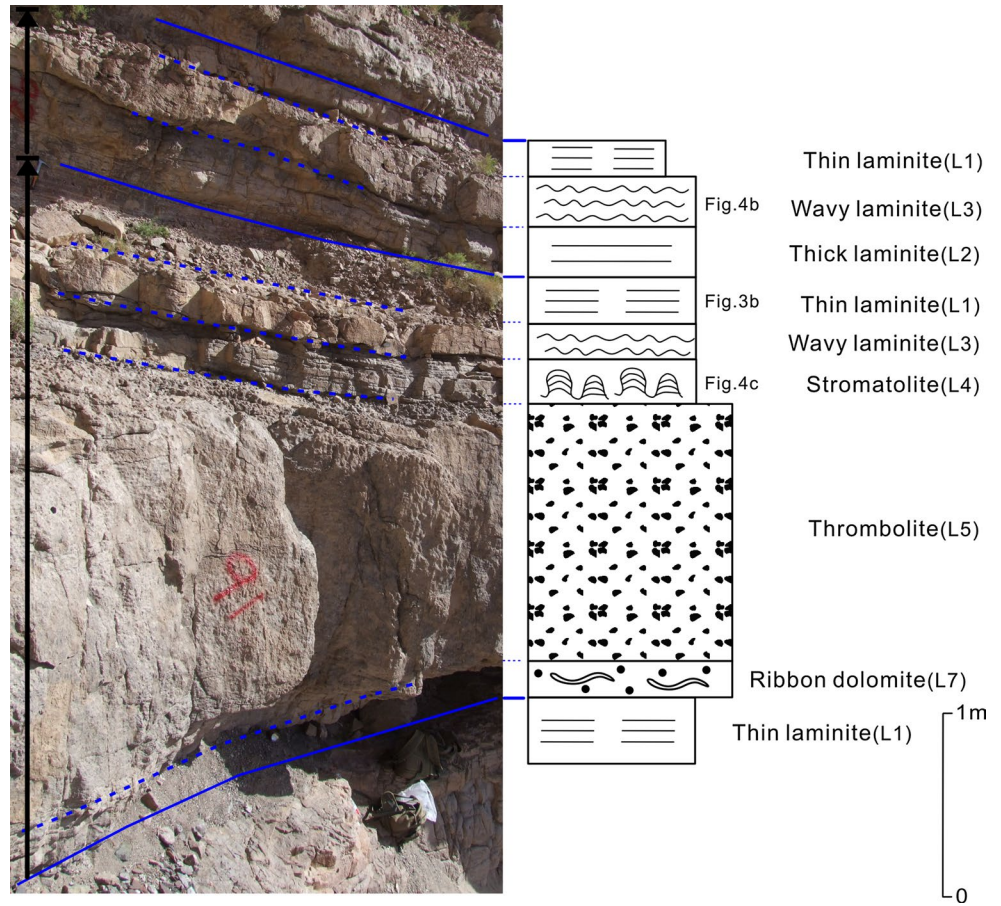


Fig. 10 a Sharp-based peritidal cycle consisting of a mounded thrombolite base (A) with fenestral peloidal wackestone/packstone intermound infill and a thick laminite (B) cap, TGL section. *Hammer* for scale (37 cm). **b** A shallow subtidal cycle that starts with

thin-bedded lenticular peloidal packstone/grainstone (L10, A), grading upwards into thick-bedded peloidal grainstone (B) and thrombotic mounds (C; within *dashed lines*), TGL section. *Arrows* mark the range of cycles. Standing person for scale (165 cm)

in asymmetrical cycles, showing a somewhat symmetrical facies arrangement within the cycles. This subtype of peritidal cycle was mostly formed in the upper part of a tidal flat (Fig. 5b) where the sea-level rise of the earliest transgression was possibly buffered (or retarded) by the fairly shallow water there, resulting in a lag effect to some extent.

Shallow subtidal cycles

Shallow subtidal cycles are commonly composed of deep to intermediate subtidal facies at their bases passing up into shallow subtidal facies. They are thus incomplete cycles in which sediments only aggraded to the shallow subtidal zones, and accommodation space was still available for deposition. These shallowing-upward cycles are typically asymmetrical cycles and generally show both thickening- and coarsening-upward trends, indicating upward increase in current energy (Fig. 10b; Koerschner and Read 1989; Osleger 1991b). Two subtypes of shallow subtidal cycle are further differentiated: one of these sub-types comprises lithofacies L10 in the basal part of the cycle, capped generally by cross-bedded L8 (Fig. 5b–B); another subtype commences with a similar basal lithofacies, but passes upward into L9 (mounded and columnar forms; Figs. 5b–A, 10b).

Origin of high-frequency, metre-scale cycles

The origin of metre-scale, shallowing-upward carbonate cycles is a matter of extensive debates, with three main mechanisms proposed: (1) Orbitally forced eustasy (Fischer 1964; Goldhammer et al. 1987, 1990, 1993; Cisneros and Vera 1993; Strasser and Hillgartner 1998), (2) Auto-cyclic processes (Ginsburg 1971; Pratt and James 1986; Chow and James 1987; Satterley 1996), and (3) jerky subsidence (Cisne 1986; Hardie and Shinn 1986; Hardie et al. 1991).

Theoretically, Milankovitch orbitally forced, high-frequency cycles would be tuned to the Earth's orbital rhythms (~20 kyr for precession, ~40 kyr for obliquity, and ~100 and 400 kyr for eccentricity (Berger et al. 1989). Such cycles may show a bundling pattern characterized by a ratio of cycles to cycle sets; for example, for Mesozoic times a ratio of 5:1 or a larger ratio of 6:1–8:1 for cycles in older rocks because of the progressive slowdown of the Earth's rotation (Berger et al. 1992; Goldhammer et al. 1993; Berger and Loutre 1994; Chen and Tucker 2003). However, it is generally difficult to determine the cycle duration from thick platform carbonate successions in view of the lack of accurate radiometric ages for a specific stratigraphic interval and the 'missed-beat effect' (Goldhammer et al. 1990). In the case of the Tarim Basin cycles, it is only possible to calculate an approximate cycle duration, based on the assumption that

the time span for the Late Cambrian (Furongian Epoch) was 10.7 Ma (from 499 to 488.3 Ma; Haq and Schutter 2008; Ogg et al. 2008). An approximate estimation of cycle duration can only be made at the continuous PLB Sect. (169 cycles), where a figure of about 63.3 kyr is obtained, which is within the Milankovitch frequency bands. If 'missed beats' (subaerial exposure and deep subtidal 'missed beats') are taken into account, the average duration of cycles would have been shorter than the estimated value. Although a hierarchy of Milankovitch rhythms is not well exhibited in the Tarim cycle stacking patterns, i.e., there are no clear cycle sets; this may have been the result of a 'missed beat effect'. The predominance of asymmetrical cycles, particularly those capped by shallow subtidal facies, is consistent with the attributes of orbitally forced eustatic sea-level fluctuations, where about 15 % of rhythm is taken up by sea-level rise and about 85 % by sea-level fall (Koerschner and Read 1989; Osleger and Read 1991; Goldhammer et al. 1993; Chen et al. 2001). This asymmetry could have been further enhanced at relatively deep (subtidal) sites during the initial rapid rise in sea-level. On the other hand, the symmetrical cycles with transgressive laminite bases were probably not formed by autogenic processes. The peritidal laminites may well have been deposited on a relatively shallow intertidal to supratidal flat during a low-amplitude, high-frequency sea-level rise, during a keep-up phase in the early transgressive part of a new cycle (Koerschner and Read 1989).

Although autogenic processes (i.e., progradation and aggradation of tidal flats and tidal channel migration) could produce shallowing-upward peritidal successions across the platform (Pratt and James 1986; Cloyd et al. 1990; Satterley 1996), they are unlikely to have been responsible for deposition of the incomplete shallow subtidal cycles. Sediment production within the carbonate factory should have been sufficient to fill any remaining accommodation space through progradation and aggradation. However, this type of cycle can be readily explained as having been formed by high-frequency fluctuations in sea-level (Goldhammer et al. 1990). In addition, it is hard to imagine that autogenic processes could have produced frequent increases in accommodation space, during the closure of the 'subtidal carbonate factory' at the end of each progradation or aggradation of a tidal flat across the platform. Thus, it is considered unlikely that the autogenic processes could have developed repetitive stacks of numerous synchronous peritidal and subtidal cycles across the Late Cambrian platform, although they may have produced some stratigraphic 'noise' in some individual cycles (Osleger and Read 1991). The widespread presence of subaerial exposure at the top of cycles does not support the autogenic mechanism either (Strasser 1991).

Although episodic jerky subsidence could have created the necessary accommodation space for deposition of shallowing-upward, metre-scale cycles (Cisne 1986; Hardie and Shinn 1986; Hardie et al. 1991), it is hard to imagine that repeated tectonic pulses over a long period time could have taken place in the relatively stable tectonic setting of the cratonic Tarim Basin. Thus, although all three mechanisms cited above could potentially generate the stratigraphic forcing necessary to create metre-scale cycles, orbitally forced, high-frequency eustatic sea-level changes are the most reasonable driving mechanism responsible for the formation of these Upper Cambrian carbonate cycles. Forward modeling has been used to provide a better understanding of the depositional controls on metre-scale cycles/parasequences, in particular whether the thickness patterns are a reflection of orbital forcing or random tectonic and autocyclic controls (Barnett et al. 2002; Burgess 2006; Dexter et al. 2009; Hill et al. 2012). Modeling has shown that with an input of regular changes in sea-level, random cycle thickness patterns can be generated, and that with random sea-level changes, ordered thickness patterns can be produced—all indicating that the recognition of Milankovitch signals in cyclic successions is not straightforward. Nevertheless, on balance it is thought that orbital forcing was the dominant control on the metre-scale cycles in the Lower Qiulitag Group. Indeed, orbital forcing has been advanced by others for Cambrian cycles elsewhere in the world (Chow and James 1987; Koerschner and Read 1989; Osleger and Read 1991; Mei et al. 2005).

Vertical stacking patterns and depositional sequences

Cycle stacking patterns and accommodation change

In shallow-water carbonate successions, the thickness of cycles, particularly of peritidal cycles, generally reflects the change in accommodation space available during a eustatic fluctuation cycle (Fischer 1964; Goldhammer et al. 1987; Read and Goldhammer 1988). Although the relationship is complicated by many factors such as quasi-periodicity of cycles, variable sedimentation rates, incomplete shallowing to sea level, non-linear subsidence rates, and ‘missed beats’ of sea-level change, these negative effects can be mitigated if additional information is included. Many studies have shown that the stacking patterns of metre-scale cycles (i.e., stratigraphic trends in cycle thickness and facies variations) in platform carbonate successions are a good reflection of variable-order stratal cyclicity controlled by high-frequency accommodation fluctuations superimposed on long-term accommodation changes (Goldhammer et al. 1990, 1993; Osleger and Read 1991; Montañez and Osleger 1993; Chen et al. 2001; Schlager 2005; Tucker and Garland

2010). These attributes bridge the link of individual metre-scale cycles to larger-scale depositional sequences (tens to hundreds of metres thick). Thus the cycle stacking patterns, including facies stacking patterns, can be used to identify larger-scale depositional sequences and their component systems tracts, especially in areas where the strata have been structurally deformed and are difficult to trace laterally.

The Fischer plot has been widely used as a graphical method to illustrate long-term accommodation changes by graphing cumulative departures from the mean cycle thickness as a function of time or cycle number (Fischer 1964; Goldhammer et al. 1987; Read and Goldhammer 1988; Sadler et al. 1993; Husineca et al. 2008; Bosence et al. 2009). A minimum of 50 cycles is recommended for this data analysis. In such a plot, thick cycle packages deviate positively from the mean cycle thickness, creating a rising limb of plots as a reflection of progressive increases in accommodation space during a relative sea-level rise. By contrast, thin cycle packages deviate negatively from the mean cycle thickness, producing a falling limb as a reflection of progressive decreases in accommodation space during the relative sea-level fall. In shallow-water carbonates with poor biostratigraphical controls, the Fischer plot thus provides a useful tool to correlate the enormously thick shallow-water carbonate successions at different widely spaced sections, mainly based on the patterns of long-term accommodation changes (or sea-level changes), with additional information including facies stacking patterns, some specific facies indicators and stratigraphic marker beds, integrated to constrain the correlations (Adams and Grotzinger 1996; Bosence et al. 2000; Chen et al. 2001).

In this study, Fischer plots were constructed by graphing cumulative departures from the mean cycle thickness against cycle thickness rather than mean cycle duration or cycle number (Chen et al. 2001). In this objective way, the Fischer plots produce similar accommodation fluctuation curves but with a more gently rising limb and steeper falling limb (Figs. 11, 12, 13, 14). In view of the dominance of peritidal cycles and absence of deeper-water subtidal cycles in the Lower Qiulitag Group, the effects of ‘missed beats’ of low-amplitude, high-frequency sea-level fluctuations in deep subtidal environments (Osleger and Read 1991; Sadler et al. 1993) are likely to be minor.

In order to assess the degree of order in the succession of cycles (Sadler et al. 1993; Lehrmann and Goldhammer 1999; Bosence et al. 2009), a statistical test (z-score) was also employed for the high-frequency cycles in the Lower Qiulitag Group (Table 2). According to Sadler et al. (1993), a z-score of less than -1.96 indicates a well-ordered stacking of cycles. The values of z-score are -1.76 - and 1.84 for the TGL and PLB sections, respectively, indicating an

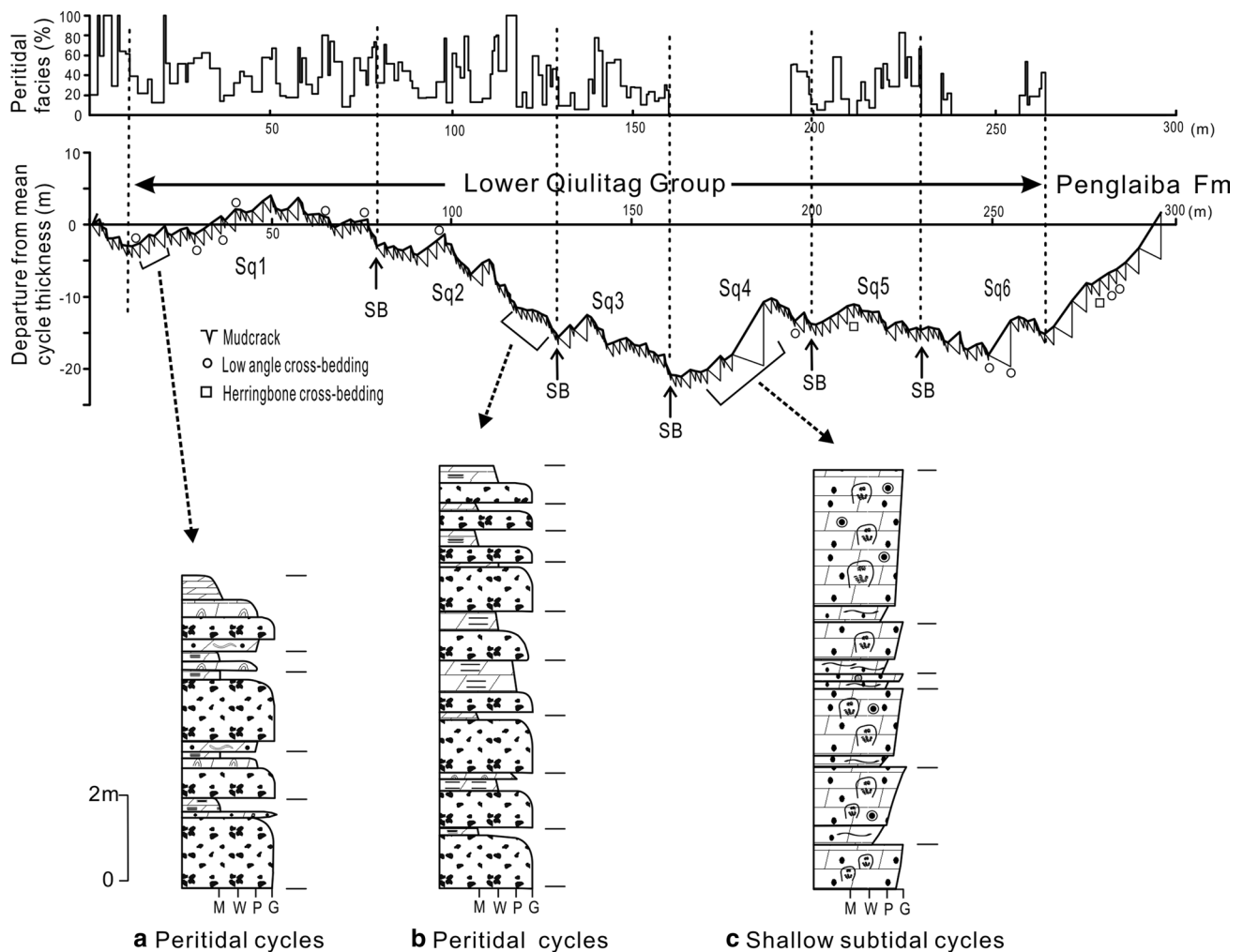


Fig. 11 Fischer plots of cycle stacking patterns and vertical facies variations (percentages of peritidal facies) in the Lower Qiulitag Group from PLB section in Aksu area. Note stacking patterns of representative metre-scale cycles: **a** Peritidal cycles formed during the third-order sea-level rise (Sq1), generally start with thin transgressive bases (ribbon peloidal packstones/grainstones), grading upwards into thick- to massive thrombolites, stromatolites and thick to thin laminites. **b** Peritidal cycles formed during the third-order sea-level

fall (Sq2), commonly consist of basal thrombolites and stromatolites/thick laminites. **c** Shallow subtidal cycles formed in an overall subtidal environment during lower-order (i.e., second-order) sea-level rise (Sq4), feature overall subtidal facies successions comprising the basal thin-bedded lenticular peloidal wackestones/grainstones capped by thick-bedded to massive peloidal-oidal grainstones and microbial buildups. *SB* sequence boundary. *Short lines on the right of logs* mark the cycle boundaries. See Fig. 5 for the legend

ordered to well-ordered vertical stacking of cycles. However, a z-score of 0.24 for the KP section probably indicates a random succession of cycles, where a non-random pattern may not be recorded with less than 50 cycles (Sadler et al. 1993).

Third-order depositional sequences

The sequence boundary surface, as indicated by long-term subaerial exposure (i.e., karstification, pedogenesis) and/or large-scale downward incision, is the key to demarcate the third-order depositional sequences (Van Wagoner et al. 1987; Vail et al. 1991; Schlager 2005). In the study area,

however, the sequence boundaries are indicated by gradational zones with higher percentages of peritidal (inter-supratidal) facies within the enormously thick succession of the Lower Qiulitag Group, composed of stacked, metre-scale, thinner-than-average cycles. Prolonged subaerial exposure indicators are generally absent at the four measured sections. Only minor mudcracks are present in the laminites (Fig. 3a) and mature paleosols are not observed at the top of cycles. Previous studies mostly favored the placement of sequence boundaries in the middle on the falling limbs of Fischer plots, representing the maximum rate of accommodation loss (Goldhammer et al. 1990; Chen et al. 2001). In this study, the sequence boundaries are placed in the lowermost point of the falling limbs within

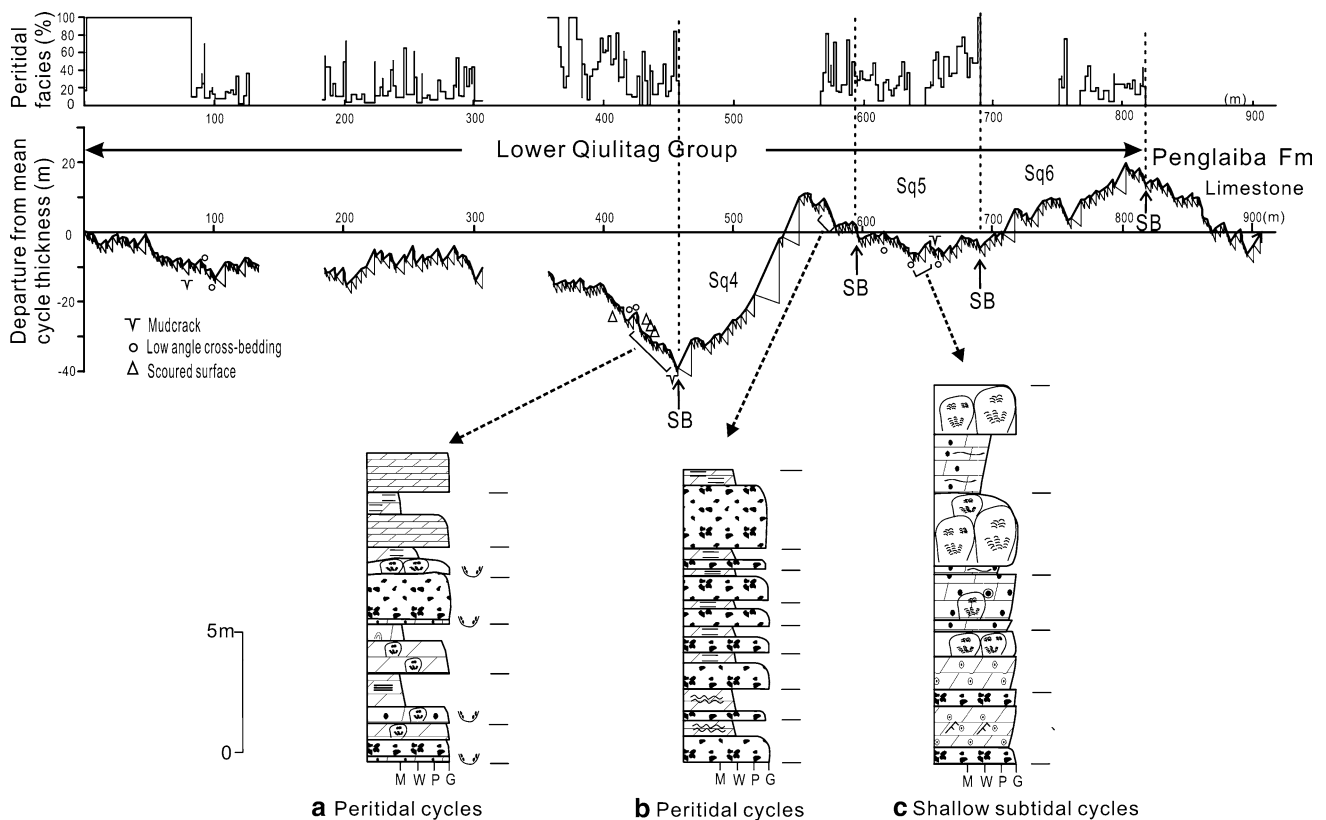


Fig. 12 Fischer plots of cycle stacking patterns and vertical facies variations in the Lower Qiulitag Group from TGL section. The stacking patterns of representative metre-scale cycles: **a** Peritidal cycles in the uppermost Sq3 formed during relative sea-level fall. **b** Peritidal cycles in the uppermost Sq4 formed during relative sea-level fall, characterized by thrombolite bases and thick laminites caps; **c** Shallow subtidal cycles in the lowermost Sq6 formed at the onset of rela-

tive sea-level rise, characterized by basal thrombolites and/or thin- to medium-bedded ooidal/peloidal grainstones capped by thick-bedded to massive peloidal grainstones and/or microbial buildups. *Gaps* on the plots are covered stratigraphic intervals in the field. *SB* sequence boundary. *Short lines* on the right of logs mark the cycle boundaries. See Fig. 5 for the legend

the gradational zones, where high percentages of intracycle peritidal facies occur (Figs. 11, 12, 13, 14). In many carbonate platform-interior successions, third-order depositional sequences commonly consist of two components in view of the weak development of the lowstand systems tract; thus each third-order sequence comprises an overall rising limb followed by a falling limb of accommodation change, with superimposed shorter-term fluctuations (Read and Goldhammer 1988; Goldhammer et al. 1990).

Six third-order depositional sequences (Sq1–Sq6), ranging from 28 to 138 m thick (average 80 m) and spanning ~1.8 Ma on average in duration, are identified on the basis of vertical facies variations (i.e., percentages of intracycle peritidal facies) and cycle stacking patterns, as revealed by Fischer plots. These sequences are relatively complete at the PLB (Fig. 11) and TGL sections (Fig. 12), but only the uppermost one (Sq6) is seen at the KP (Fig. 13) and YAB sections (Fig. 14) because of limited stratal exposure. In general, they consist of a higher ratio of shallow subtidal facies in a thickening-up lower part,

and a peritidal facies-dominated, thinning-up upper part, in which the internal shallowing-upward cycles are quite variable in cycle number (16–52 cycles) at different localities. These sequences can be further grouped into larger-scale sequence sets: the lower sequence set (Sq1–Sq3) and the upper sequence set (Sq4–Sq6; Fig. 15).

Sequences Sq1–Sq3: these sequences characterize an overall falling slope in the Fischer plots (Fig. 15), indicating a long-term cumulative, although episodic, decrease in accommodation space. Peritidal facies overwhelmingly predominate in these sequences, even in the lower part of the sequences (Figs. 11, 12). Sequence Sq1 is composed of thicker-than-average peritidal cycles. The cycle package in the lower transgressive part of Sq1, although being composed of peritidal cycles as well, covers the most complete spectrum from the restricted shallow subtidal to supratidal facies, commonly with a thin ribbon dolomite (L7) at the base (Figs. 9, 11a); the cycle package in the upper regressive part, however, generally does not have ribbon dolomite (L7) bases and thrombolite (L5) occurs there. Similar

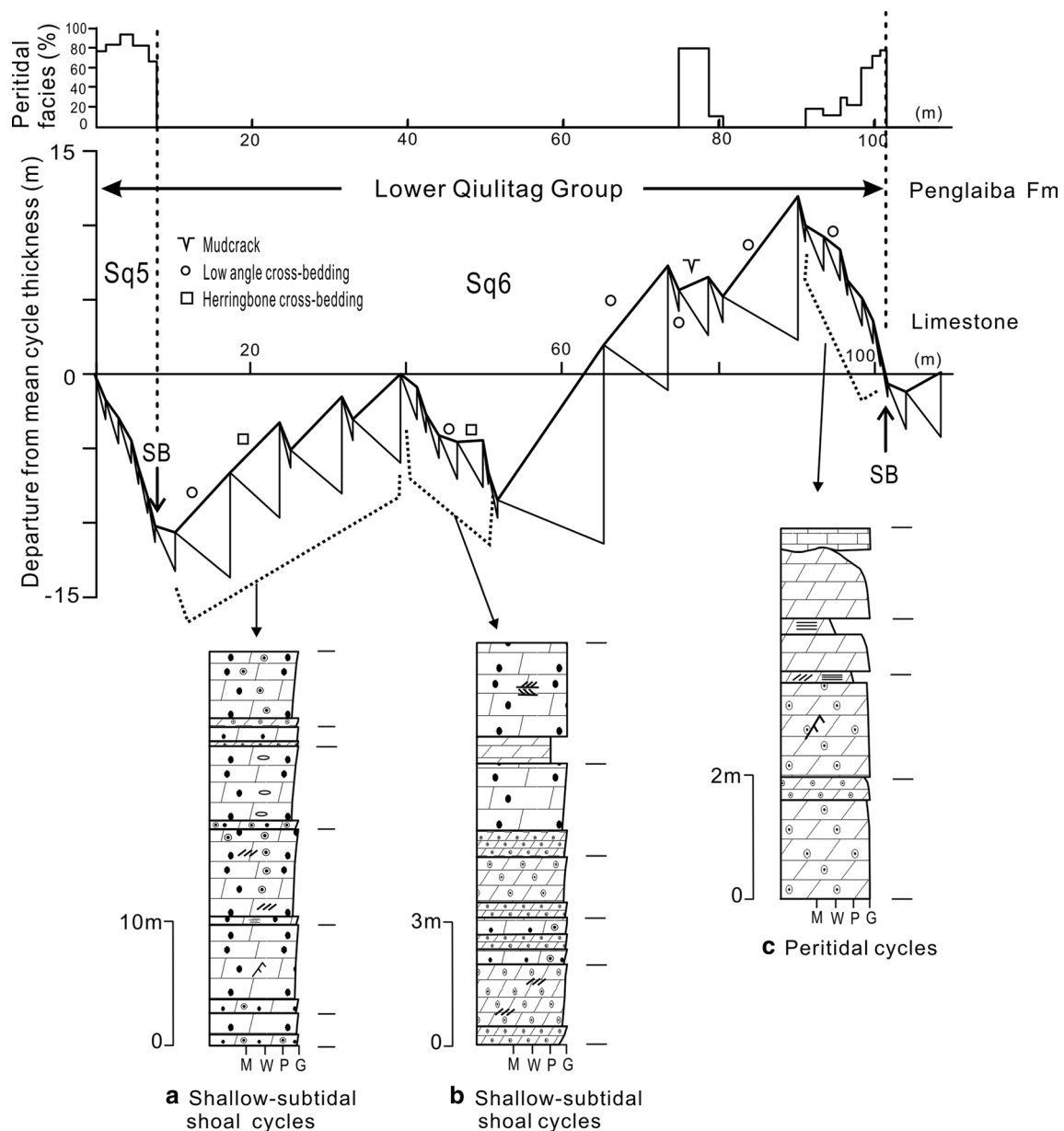


Fig. 13 Fischer plots of cycle stacking patterns and *vertical* facies variations in the uppermost Lower Qiulitag Group from KP section where shallow subtidal shoal cycles predominate over most of

studied interval (**a**, **b**), and peritidal cycles only occur near the top of sequence boundary (**c**). *SB* sequence boundary. Refer to Fig. 5 for legend

patterns are found in Sq2 (Fig. 11b). In contrast, sequence Sq3 comprises thinner-than-average peritidal cycles with increased evidence of subaerial exposure at the tops of cycles, particularly in the upper part (Fig. 12a). The basal thrombolites (L5) become thinner even in the lower part (e.g., Fig. 10a), indicating a significant overall decrease in accommodation space.

Sequences Sq4 to Sq6: These sequences characterize a rising trend of plots in the upper part of the Lower Qiulitag Group (Fig. 15), indicating a long-term accommodation increase, although episodic. In comparison

to the lower sequence set (Sq1–Sq3), these sequences are dominated by shallow subtidal facies (i.e., L8 and L9; Figs. 10b, 11, 12, 13, 14), even in the upper parts of some sequences (Fig. 13), so that they are composed mainly of thicker cycles which reach 18 m thick locally (Figs. 11, 12). Therefore, cycle numbers of each sequence generally decrease (Fig. 15). This scenario may have resulted from the ‘missed beats’ of low-amplitude, high-frequency sea-level fluctuations in the deep subtidal environments (Goldhammer et al. 1990; Osleger and Read 1991).

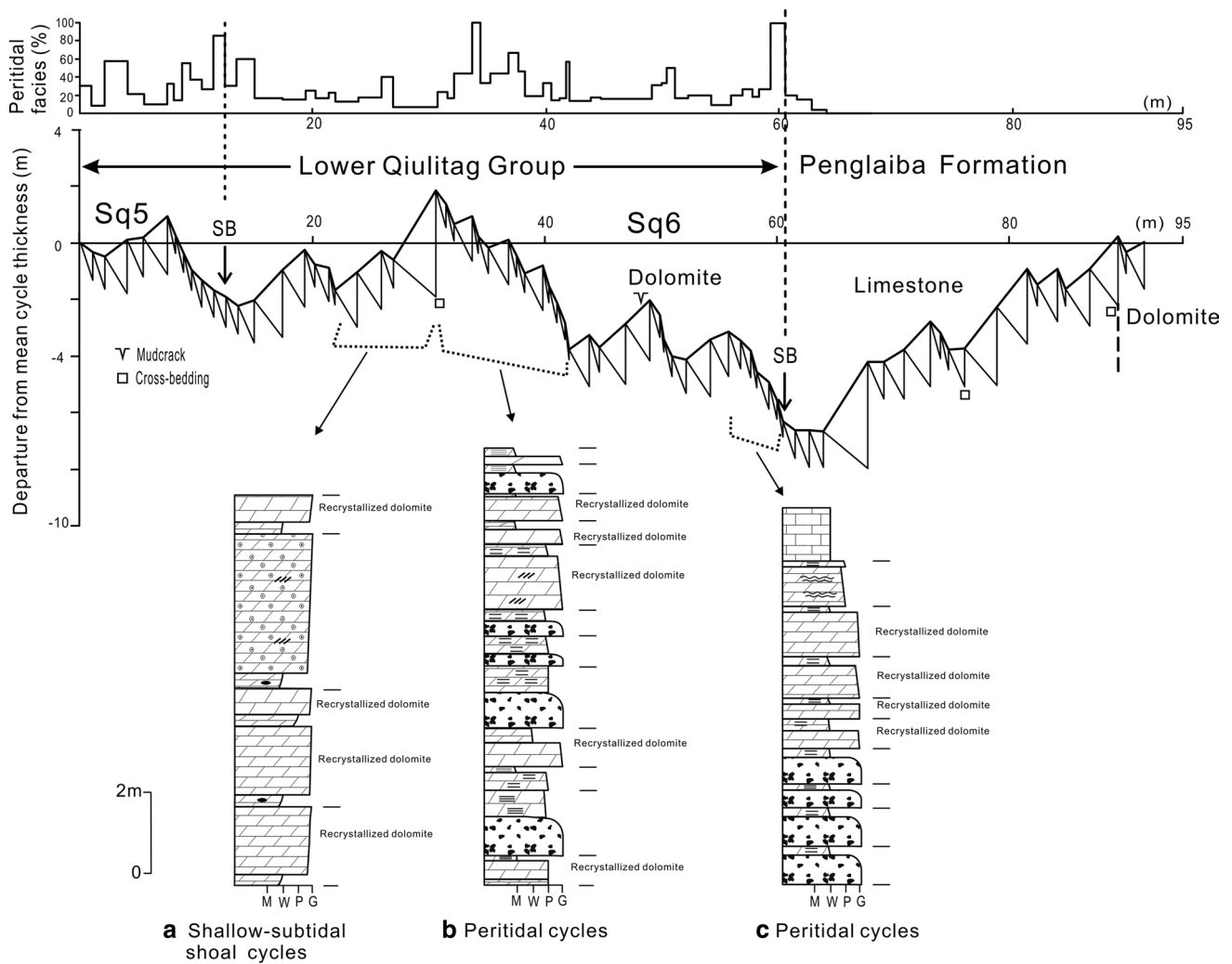


Fig. 14 Fischer plots of cycle stacking patterns and vertical facies variations in the uppermost Lower Qiulitag Group from YAB section. Compared to the KP section Fischer plots, shallow subtidal cycles only occur in the lower part of sequence (a), whereas peritidal cycles

predominate over the upper part of the sequence (b, c), indicating shallowing somewhat in deposition. SB sequence boundary. Refer to Fig. 5 for legend

Table 2 Z-scores for successions of metre scale cycles in four sections of NW Tarim Basin

Section	No. cycles	Average thickness	$n1>$	$n2<$	r (runs)	Z score
PLB	188	1.57	72	116	77	-1.84
TGL	338	2.39	122	216	142	-1.76
KP	36	3.01	10	26	16	0.24
YAB	70	1.31	27	43	32	-0.55

$n1>$ is the number of thick cycles (thicker than the average); $n2<$ is the number of thin cycles (thinner than average); r is the number of runs

Correlation of depositional sequences in the Upper Cambrian and controls on platform development

Many studies of Cambrian sequences have been undertaken in the Tarim Basin. However, different conclusions have been drawn from the identification of third-order

depositional sequences in the Lower Qiulitag Group (Upper Cambrian) carbonates. Based mainly on outcrop investigations, Yu et al. (1996, 2001) recognized seven third-order sequences from the northern Tarim platform. Gao et al. (2006) identified three third-order sequences on the basis of field observations and carbon isotope

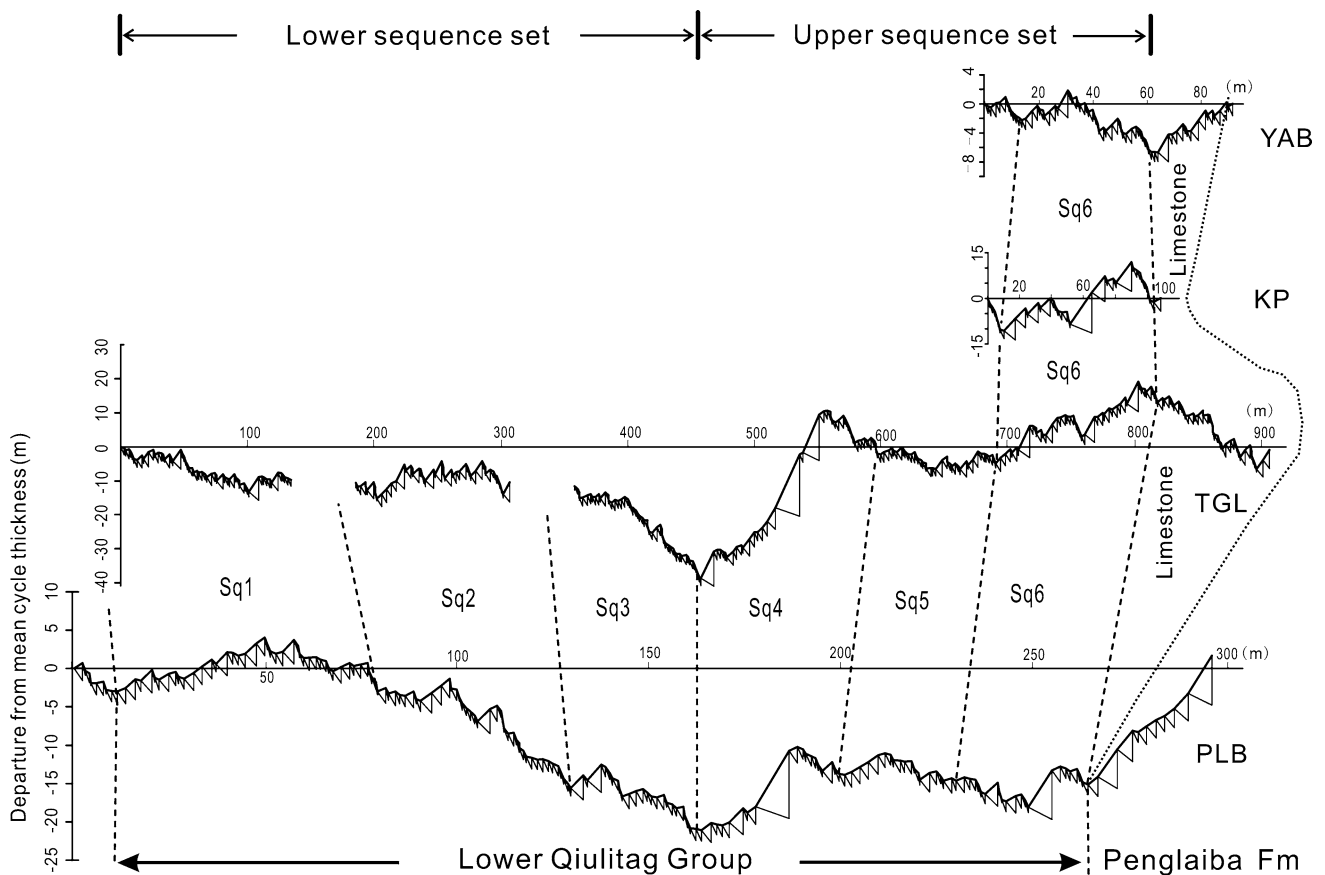


Fig. 15 Correlation of Fischer plots for the Lower Qiulitag Group of Upper Cambrian from four measured sections (see Fig. 1 for location) in northwestern Tarim Basin. Six third-order sequences (Sq1–Sq6) are identified at PLB and TGL sections. Only the uppermost

Sq6 is present at KP and YAB sections because of incomplete exposure. Sequence stacking patterns reveal a synoptic accommodation (or sea-level) decrease from Sq1 to Sq3 and an increase from Sq4 to Sq6, defining two sequence sets

chemostratigraphy from borehole logs in the Keping-Bachu-Tazhong region. Zhao et al. (2010) recognized two depositional sequences, mainly based on field studies, seismic reflection data and borehole logs, which likely correspond to the two sequence sets of this study. Chen et al. (1999) only distinguished one sequence in the Aksu-Bachu area on the basis of field investigations. These inconsistent results from different researchers may result from which the apparent vertical and lateral facies changes (terminations and/or progradation) across the sequence boundaries, as seen in the conventional sequence model (Vail et al. 1991), are difficult to observe and trace in thick, cyclic platform carbonate successions.

Previous biostratigraphic studies suggested that the Lower Qiulitag Group was roughly constrained within the Upper Cambrian (or Furongian), although not exactly defined for the lower and upper boundaries (Fig. 2; Zhou et al. 1991; Zhang and Gao 1992; Zhou 2001). Traditionally, this formation is separated from the overlying Lower Ordovician Penglaiba Formation by the first occurrence of light grey limestones (Fig. 2), which can be easily

recognized in the field and traced a long distance from satellite images (Fig. S1). In this study, six third-order sequences were identified in the thick dolomite successions of the Lower Qiulitag Group in the NW Tarim based on detailed field investigations, vertical facies (percentages of intracycle peritidal facies) and cycle stacking patterns as revealed by Fischer plots (Fig. 15). Within equivalent stratigraphic successions, these sequences can be correlated with those in North China (Shi et al. 1997), North America (Koerschner and Read 1989; Read 1989; Osleger 1991a; Osleger and Read 1991) and likely elsewhere around the world (Fig. 16; Haq and Schutter 2008). This scenario suggests a major control in particular, of third-order, eustatic changes on deposition of the Upper Cambrian carbonate sequences in the Tarim Basin, although lithofacies may vary in different areas due to regional tectonics, platform morphology, sediment supply, climate and short-term sea-level changes. In turn, this scenario further improves the previous stratigraphic classification of the Lower Qiulitag Group within the Upper Cambrian in the Tarim Basin. At the PLB section, however, it should be noted that the limestone marker

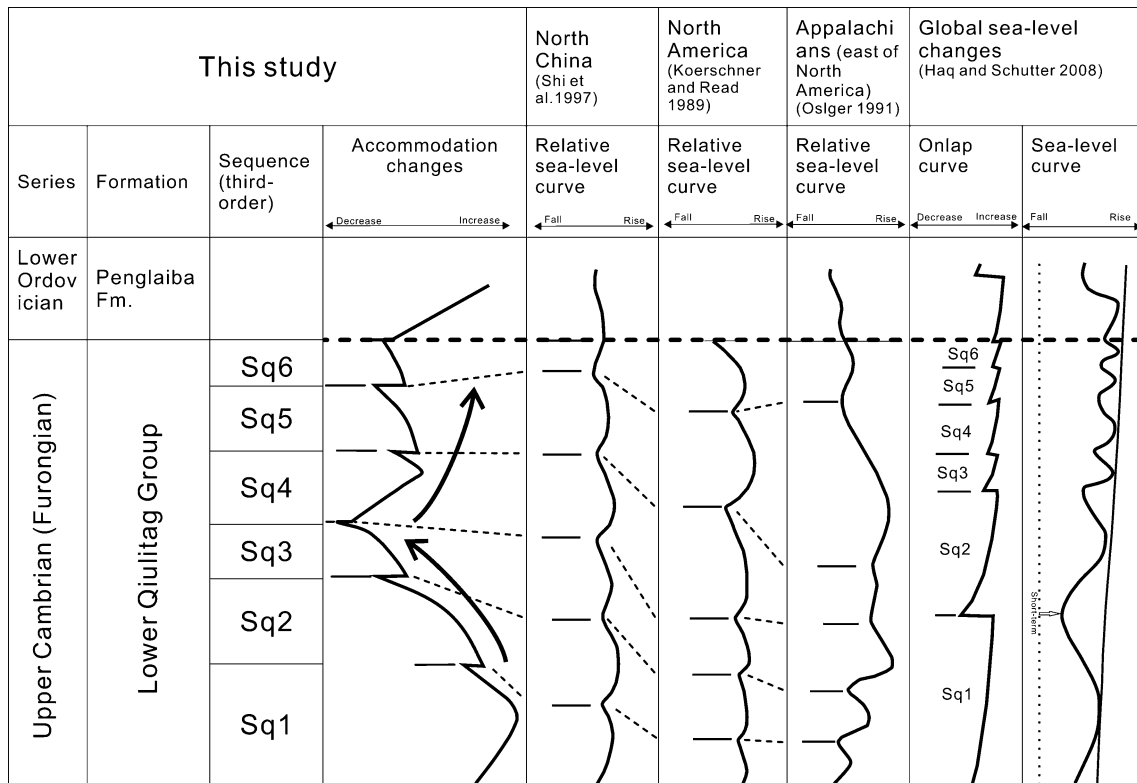


Fig. 16 Correlation of third-order sequences in the Upper Cambrian and concomitant accommodation (or sea-level) changes in the study area with those of carbonate platforms elsewhere around the world. Six third-order depositional sequences and relevant sea-level fluctuations recognized from the Lower Qiulitag Group are correlated with

equivalents on other carbonate platforms. A longer-term decrease in accommodation space from Sq1 to Sq3 and subsequent increase from Sq4 to Sq6, reflects a longer-term synoptic sea-level fall, then a rise (arrows) during the Late Cambrian

bed used to demarcate this stratigraphic unit from the overlying Penglaiba Formation has been altered through burial dolomitization (Fig. 11), rendering correlations somewhat uncertain. However, the cycle stacking patterns revealed in this study provide a useful independent constraint to place the Cambrian-Ordovician boundary in the platform successions of the Tarim Basin through matching the cycle and sequence patterns elsewhere (Fig. 15).

The larger-scale sequence stacking patterns show a longer-term (second-order) decrease in accommodation space from Sq1 to Sq3 and subsequent increase from Sq4 to Sq6, reflecting a longer-term (second-order) synoptic sea-level fall, then a rise on which third-order sea-level fluctuations were superimposed during the Late Cambrian (Figs. 15, 16). This scenario is different from the longer-term patterns of sea-level changes elsewhere (Koerschner and Read 1989; Haq and Schutter 2008), and this is likely to have resulted from a different tectonic history from other areas.

Lateral facies variations within the sequence framework across the studied sections show that the open-marine subtidal facies, mainly lithofacies L8, L9 and L10 (Fig. 5),

predominate at the KP and TGL sections (Figs. 12, 13), suggesting that an open-marine intraplatform (or intrashelf) bay or depression developed at the two localities and extended northwestward to link with the Tianshan Ocean (Fig. 5a). An increased subsidence rate could have resulted in a higher depositional rate there, thereby accommodating a thicker carbonate succession, about twice as thick as surrounding sites (i.e., 297 m thick at the PLB vs. 761 m thick at the TGL section; Fig. 15).

Conclusions

Detailed studies of facies, high-frequency cyclostratigraphy and sequence stratigraphy of the Lower Qiulitag Group (Upper Cambrian) composed exclusively of dolomites at four outcrop sections in the NW Tarim Basin show that:

Based on the lithology and sedimentary structures, ten lithofacies (L1–L10) are identified, which are interpreted to have been deposited in intermediate to shallow subtidal, to restricted shallow subtidal, to intertidal and supratidal environments on a carbonate ramp system.

Two main types of metre-scale, shallowing-upward cycles are recognized: subtidal and peritidal cycles. Peritidal cycles of intertidal-supratidal facies are predominant especially in the lower part of the Lower Qiulitag Group in which thrombolite-based cycles are the most common. Shallow subtidal cycles are less common, and occur mainly in the upper part of the Lower Qiulitag Group. Several subtypes are further differentiated based on the basal facies components.

Six third-order depositional sequences (Sq1–Sq6) are distinguished and are generally composed of two parts: a lower thicker, shallow subtidal facies-dominant succession, and an upper thinner, peritidal facies-dominant succession. Sequence boundaries are generally gradational and conformable stratigraphic intervals, as shown by stacked and thinner-than-average cycle zones on Fischer plots, rather than by a single boundary surface subject to prolonged sub-aerial exposure during a major sea-level fall.

The identified depositional sequences are correlated well with those in coeval Upper Cambrian successions elsewhere in the world, indicating a third-order eustatic control on the deposition of these sequences. The high-frequency, metre-scale, and shallowing-upward cycles were likely formed in response to high-frequency eustatic sea-level fluctuations which were superimposed on third-order sea-level changes. The larger-scale sequence sets indicate that these sequences were also controlled by longer-term sea-level changes likely induced by the tectonic evolution of the Tarim Basin. Differential tectonic subsidence on the carbonate platform further controlled the spatial distribution of the various facies and depositional rate.

Acknowledgments This work was funded by National Science and Technology Special Project of China (grant no. 2011ZX0500803) and National Basic Research Project (973 Project grant no. 2012CB214802). Thanks go to Nancy Chow and two anonymous reviewers for their critical and constructive comments in the previous version and to the Chief Editor Maurice Tucker for his patience in handling this paper, inspiring comments and editorial works, all of which improved the manuscript significantly.

References

Adams RD, Grotzinger JP (1996) Lateral continuity of facies and parasequences in Middle Cambrian platform carbonates, Carrara Formation, southeastern California, USA. *J Sediment Res* 66:1079–1090

Aitken J (1967) Classification and environmental significance of cryptalgal limestones and dolomites, with illustrations from the Cambrian and Ordovician of southwestern Alberta. *J Sediment Res* 37:1163–1178

Barnett A, Burgess PM, Wright VP (2002) Icehouse world sea-level behaviour and resulting stratal patterns in late Visean (Mississippian) carbonate platforms: integration of numerical forward modelling and outcrop studies. *Basin Res* 14:417–438

Berger A, Loutre M (1994) The climate of the next 100,000 years. *Le Temps en Géologie: du Passé au Futur, Actes du Colloque Géoprospective-Paris*. Unesco, Paris, pp 69–76

Berger A, Loutre M, Dehant V (1989) Astronomical frequencies for pre-Quaternary palaeoclimate studies. *Terra Nova* 1:474–479

Berger A, Loutre M, Laskar J (1992) Stability of the astronomical frequencies over the Earth's history for paleoclimate studies. *Science* 255:560–566

Bosence DWJ, Wood JL, Rose EPF, Qing H (2000) Low- and high-frequency sea-level changes control peritidal carbonate cycles, facies and dolomitization in the Rock of Gibraltar (Early Jurassic, Iberian Peninsula). *J Geol Soc* 157:61–74

Bosence D, Procter E, Aurell M, Bel Kahla A, Boudagher-Fadel M, Casaglia F, Cirilli S, Mehdie M, Nieto L, Rey J et al (2009) A dominant tectonic signal in high-frequency, peritidal carbonate cycles? A regional analysis of Liassic platforms from Western Tethys. *J Sediment Res* 79:389–415

Burgess PM (2006) The signal and the noise: forward modeling of allocyclic and autocyclic processes influencing peritidal carbonate stacking patterns. *J Sediment Res* 76:962–977

Chen DZ, Tucker ME (2003) The Frasnian–Famennian mass extinction: insights from high-resolution sequence stratigraphy and cyclostratigraphy in South China. *Palaeogeogr Palaeoclimatol Palaeoecol* 193:87–111

Chen DZ, Tucker ME, Jiang MS, Zhu JQ (2001) Long-distance correlation between tectonic-controlled, isolated carbonate platforms by cyclostratigraphy and sequence stratigraphy in the Devonian of South China. *Sedimentology* 48:57–78

Chen GJ, Xue LH, Wang Q, Kang J, Xiao LX, Shi J (1999) Sea-level changes and formation of cyclic sequence of Cambrian–Ordovician in Akesu–Bachu Area, Xinjiang. *Acta Sedimentol Sin* 17:192–197 (in Chinese with English abstract)

Chen XJ, Cai XY, Xu XH (2006) The research on sedimentation features in Cambrian–Ordovician sequence frame in the center of Tarim. *Xinjiang Geol* 24:276–280 (in Chinese with English abstract)

Chow N, James NP (1987) Cambrian grand cycles: a northern Appalachian perspective. *Bull Geol Soc Am* 98:418–429

Cisne JL (1986) Earthquakes recorded stratigraphically on carbonate platforms. *Nature* 323:320–322

Cisneros CJ, Vera J (1993) Milankovitch cyclicity in Purbeck peritidal limestones of the Prebetic (Berriasian, southern Spain). *Sedimentology* 40:513–537

Cloyd KC, Demicco RV, Spencer RJ (1990) Tidal channel, levee, and crevasse-splay deposits from a Cambrian tidal channel system; a new mechanism to produce shallowing-upward sequences. *J Sediment Res* 60:73–83

Demicco RV (1983) Wavy and lenticular-bedded carbonate ribbon rocks of the Upper Cambrian Conococheague Limestone, central Appalachians. *J Sediment Res* 53:1121–1132

Demicco RV (1985) Platform and off-platform carbonates of the Upper Cambrian of western Maryland, USA. *Sedimentology* 32:1–22

Demicco RV, Hardie LA (1994) Sedimentary structures and early diagenetic features of shallow marine carbonate deposits. *SEPM (Society of Sedimentary Geology)*, p 255

Dexter TA, Kowalewski M, Read JF (2009) Distinguishing Milankovitch-driven processes in the rock record from stochasticity using computer-simulated stratigraphy. *J Geol* 117:349–361

Dunham RJ (1962) Classification of carbonate rocks according to depositional texture. In: Ham WE (ed) *Classification of carbonate rocks*. AAPG Mem 1:108–121

Elrick M (1995) Cyclostratigraphy of Middle Devonian carbonates of the eastern Great Basin. *J Sediment Res* 65:61–79

- Fan TL, Yu BS, Gao ZQ (2007) Characteristics of carbonate sequence stratigraphy and its control on oil-gas in Tarim Basin. *Geoscience* 21:57–65 (in Chinese with English abstract)
- Feldmann M, McKenzie JA (1998) Stromatolite-thrombolite associations in a modern environment, Lee Stocking Island, Bahamas. *Palaios* 13:201–212
- Fischer AG (1964) The Lofer cyclothems of the alpine Triassic. In: Merriam DF (ed) *Symposium on Cyclic Sedimentation*. Kansas State Geol Surv Bull 169:107–149
- Fischer AG, Bottjer DJ (1991) Orbital forcing and sedimentary sequences. *J Sediment Petrol* 61:1063–1069
- Gao ZQ, Fan TL, Li Y, Liu WH, Chen YL (2006) Study on eustatic sea level change rule in Cambrian–Ordovician in Tarim Basin. *J Jilin Univ (Earth Sci Ed)* 36:549–556 (in Chinese with English abstract)
- Ginsburg RN (1971) Landward movement of carbonate mud: new model for regressive cycles in carbonates: abstract. *AAPG Bull* 55:340
- Ginsburg RN (1975) *Tidal deposits: a casebook of recent examples and fossil counterparts*. Springer, p 428
- Glumac B, Walker KR (2000) Carbonate deposition and sequence stratigraphy of the terminal Cambrian grand cycle in the southern Appalachians, USA. *J Sediment Res* 70:952–963
- Goldhammer RK, Dunn PA, Hardie LA (1987) High-frequency glacio-eustatic sea-level oscillations with Milankovitch characteristics recorded in Middle Triassic platform carbonates in northern Italy. *Am J Sci* 287:853–892
- Goldhammer RK, Dunn PA, Hardie LA (1990) Depositional cycles, composite sea-level changes, cycle stacking patterns, and the hierarchy of stratigraphic forcing: examples from Alpine Triassic platform carbonates. *Geol Soc Am Bull* 102:535–562
- Goldhammer RK, Lehmann PJ, Dunn PA (1993) The origin of high-frequency platform carbonate cycles and third-order sequences (Lower Ordovician El Paso Gp, West Texas): constraints from outcrop data and stratigraphic modeling. *J Sediment Res* 63:318–359
- Haq BU, Schutter SR (2008) A chronology of Paleozoic sea-level changes. *Science* 322:64–68
- Hardie LA, Shinn EA (1986) Carbonate depositional environments, modern and ancient: part 3: Tidal flats. *Colo Sch Mines Q* 81:1–74
- Hardie LA, Dunn PA, Goldhammer RK (1991) Field and modelling studies of Cambrian carbonate cycles, Virginia Appalachians; discussion. *J Sediment Petrol* 61:636–646
- Hill J, Wood R, Curtis A, Tetzlaff DM (2012) Preservation of forcing signals in shallow water carbonate sediments. *Sed Geol* 275:79–92
- Hofmann MH, Keller M (2006) Sequence stratigraphy and carbonate platform organization of the Devonian Santa Lucia Formation, Cantabrian Mountains, NW-Spain. *Facies* 52:149–167
- Hofmann A, Dirks PHGM, Jelsma HA (2004) Shallowing-upward carbonate cycles in the Belingwe Greenstone Belt, Zimbabwe: a record of Archean sea-level oscillations. *J Sediment Res* 74:64–81
- Husineca A, Basch D, Rose B, Read JF (2008) FISCHERPLOTS: an Excel spreadsheet for computing Fischer plots of accommodation change in cyclic carbonate successions in both the time and depth domains. *Comput Geosci* 34:269–277
- Jia CZ, Wei GQ (2002) Structural characteristics and petroliferous features of Tarim Basin. *Chin Sci Bull* 47:1–11
- Jia CZ, Zhang SB (2004) Wu SZ (2004) *Stratigraphy of the Tarim Basin and adjacent areas*. Science Press, Beijing, p 1063 (in Chinese)
- Kang YZ, Kang ZH (1996) Tectonic evolution and oil and gas of Tarim basin. *J Southeast Asian Earth Sci* 13:317–325
- Kennard JM, James NP (1986) Thrombolites and stromatolites; two distinct types of microbial structures. *Palaios* 1:492–503
- Koerschner WF, Read JF (1989) Field and modelling studies of Cambrian carbonate cycles, Virginia, Appalachians. *J Sediment Res* 59:654–687
- Laya JC, Tucker ME, Perez-Huerta A (2013) Metre-scale cyclicity in Permian ramp carbonates of equatorial Pangea (Venezuelan Andes): implications for sedimentation under tropical Pangea conditions. *Sedimentary Geology* 292:15–35
- Lee JH, Chen J, Chough S (2010) Paleoenvironmental implications of an extensive maceriate microbialite bed in the Furongian Chaomidian Formation, Shandong Province, China. *Palaeogeogr Palaeoclimatol Palaeoecol* 297:621–632
- Lehrmann DJ, Goldhammer RK (1999) Secular variation in parasequence and facies stacking patterns of platform carbonates: a guide to application of stacking-patterns analysis in strata of diverse ages and settings. In: Harris PM, Saller AH, Simo JA (eds) *Advances in sequence stratigraphy: Applications to reservoir, outcrops, and models*. vol 63. SEPM Special Publication, pp 187–226
- Li DS, Liang DG, Jia CZ, Wang G, Wu QZ, He DF (1996) Hydrocarbon accumulations in the Tarim basin, China. *AAPG Bull* 80:1587–1603
- Lin CS, Yang HJ, Liu JY, Rui ZF, Cai ZZ, Li ST, Yu BS (2011) Sequence architecture and depositional evolution of the Ordovician carbonate platform margins in the Tarim Basin and its response to tectonism and sea-level change. *Basin Res* 24:1–24
- Mei MX, Ma YS, Deng J, Chen HJ (2005) From cycles to sequences: sequence stratigraphy and relative sea level change for the Late Cambrian of the North China Platform. *Acta Geol Sin-Engl Ed* 79:372–383
- Meng X, Ge M, Tucker ME (1997) Sequence stratigraphy, sea-level changes and depositional systems in the Cambro-Ordovician of the North China carbonate platform. *Sediment Geol* 114:189–222
- Montañez IP, Osleger DA (1993) Parasequence stacking patterns, third-order accommodation events, and sequence stratigraphy of Middle to Upper Cambrian platform carbonates, Bonanza King Formation, southern Great Basin. In: Loucks B, Sarg JF (eds) *Recent advances and applications of carbonate sequence stratigraphy*, vol 57. AAPG Memoir, pp 305–326
- Mutti M, Simo J (1993) Stratigraphic patterns and cycle-related diagenesis of upper Yates Formation, Permian, Guadalupe mountains. In: Loucks B, Sarg JF (eds) *Recent advances and applications of carbonate sequence stratigraphy*, vol 57. AAPG Memoir, pp 515–534
- Ogg JG, Ogg G, Gradstein F (2008) *The concise geologic time scale*. Cambridge University Press, Cambridge p, p 184
- Osleger DA (1991a) Cyclostratigraphy of Late Cambrian carbonate sequences: an interbasinal comparison of the Cordilleran and Appalachian passive margins. *Paleozoic Paleogeography of the Western United States II Pacific Section, Society of Economic Paleontologists and Mineralogists Field Trip Guidebook* 67: 811–828
- Osleger DA (1991b) Subtidal carbonate cycles: implications for allo-cyclic vs. autocyclic controls. *Geology* 19:917–920
- Osleger DA, Read JF (1991) Relation of eustasy to stacking patterns of metre-scale carbonate cycles, late Cambrian, USA. *J Sediment Res* 61:1225–1252
- Osleger DA, Read JF (1993) Comparative analysis of methods used to define eustatic variations in outcrop: late Cambrian interbasinal sequence development. *Am J Sci* 293:157–216
- Pratt BR, James NP (1986) The St George Group (Lower Ordovician) of western Newfoundland: tidal flat island model for carbonate sedimentation in shallow epeiric seas. *Sedimentology* 33:313–343

- Pratt BR, James N, Cowan C (1992) Peritidal carbonates. In: Walker RG, James N (eds) *Facies models: response to sea level change*. Geological Association of Canada, *GeoText* 1, pp 303–322
- Read JF (1989) Controls on evolution of Cambrian-Ordovician passive margin, US Appalachians. In: Crevello PD, Wilson JL, Sarg JF, Read JF (eds) *Controls on Carbonate Platform and Basin Development*. SEPM, Special Publication 44:147–165
- Read JF, Goldhammer RK (1988) Use of Fischer plots to define third-order sea-level curves in Ordovician peritidal cyclic carbonates, Appalachians. *Geology* 16:895–899
- Read JF, Repetski JE (2012) Cambrian–lower Middle Ordovician passive carbonate margin, southern Appalachians. In: Derby JR, Fritz JR, Longacre SA, Morgan WA, Sterbach CA (eds) *The great American carbonate bank: the geology and economic resources of the Cambrian-Ordovician Sauk megasequence of Laurentia*. AAPG Mem 98:357–382
- Riding R (2000) Microbial carbonates: the geological record of calcified bacterial–algal mats and biofilms. *Sedimentology* 47(Suppl. 1):179–214
- Sadler PM, Osleger DA, Montanez IP (1993) On the labeling, length, and objective basis of Fischer plots. *J Sediment Res* 63:360–368
- Satterley AK (1996) Cyclic carbonate sedimentation in the Upper Triassic Dachstein Limestone, Austria; the role of patterns of sediment supply and tectonics in a platform-reef-basin system. *J Sediment Res* 66:307–323
- Schlager W (2005) Carbonate sedimentology and sequence stratigraphy. SEPM concepts in sedimentology and paleontology, vol 8, p 208
- Shapiro RS (2000) A comment on the systematic confusion of thrombolites. *Palaios* 15:166–169
- Sherman A, Narbonne G, James N (2001) Anatomy of a cyclically packaged Mesoproterozoic carbonate ramp in northern Canada. *Sediment Geol* 139:171–203
- Shi XY, Chen JQ, Mei SL (1997) Cambrian sequence chronostratigraphic framework of the North China Platform. *Earth Sci Front* 4:161–173 (in Chinese with English abstract)
- Shinn EA (1983) Tidal flat environment. In: Scholl PA, Bebout DG, Moore CH (eds) *Carbonate depositional environments*. AAPG Mem 33:172–210
- Strasser A (1991) Lagoonal-peritidal sequences in carbonate environments: autocyclic and allocyclic processes. In: Einsele G, Ricken W, Seilacher A (eds) *Cycles and events in stratigraphy*. Springer, Berlin, pp 709–721
- Strasser A, Hillgärtner H (1998) High-frequency sea-level fluctuations recorded on a shallow carbonate platform (Berriasian and Lower Valanginian of Mount Salève, French Jura). *Eclogae Geol Helv* 91:375–390
- Strasser A, Hillgärtner H, Hug W, Pittet B (2000) Third-order depositional sequences reflecting Milankovitch cyclicality. *Terra Nova* 12:303–311
- Tucker ME, Garland J (2010) High-frequency cycles and their sequence stratigraphic context: orbital forcing and tectonic controls on Devonian cyclicality, Belgium (The André Dumont medalist lecture). *Geol Belg* 13:213–240
- Tucker ME, Wright VP, Dickson JAD (1990) *Carbonate Sedimentology*. Blackwell Science, Oxford, p 482
- Vail PR, Audemard F, Bowman S, Eisner P, Pérez C (1991) The stratigraphic signatures of tectonics, eustasy and sedimentology—an overview. In: Einsele G, Ricken W, Seilacher A (eds) *Cycles and events in stratigraphy*. Springer, Berlin, pp 617–659
- Van Wagoner JC, Mitchum RM, Posamentier HW, Vail PR (1987) Seismic stratigraphy interpretation using sequence stratigraphy, part 2: key definitions of sequence stratigraphy. In: Bally AW (ed) *Atlas of seismic stratigraphy*, vol 27. AAPG Studies in Geology, pp 1–10
- Wright VP, Burchette TP (1996) Shallow-water carbonate environments sedimentary environments. In: Reading HG (ed) *Sedimentary environments: processes, facies and stratigraphy*. Blackwell Science, Oxford, pp 325–394
- Yang YJ, Liu JD (2011) Sequence lithofacies paleogeography of Cambrian in Tarim Basin. *Nat Gas Geosci* 22:450–459 (in Chinese with English abstract)
- Yu BS (1996) The sequence chronostratigraphy of Cambrian-Ordovician in the Northern Tarim Basin. *Geosciences* 10:93–98 (in Chinese with English abstract)
- Yu BS, Chen JQ, Lin CS (2001) Cambrian-Ordovician sequence stratigraphy on the northern Tarim Platform and its correlation with Yangtze Platform and North China Platform. *Sci China Ser D-Earth Sci* 44:373–384
- Zhang SB, Gao QQ (1992) Sinian to Permian stratigraphy and palaeontology of the Tarim Basin. Kalpin-Bachu Region Xinjiang. The Petroleum Industry Press, Beijing, p 329 (in Chinese with English abstract)
- Zhao ZJ, Zhang YB, Pan M, Wu XN, Pan WQ (2010) Cambrian sequence stratigraphic framework in Tarim Basin. *Geol Rev* 56:609–620 (in Chinese with English abstract)
- Zheng HR, Wu MB, Wu XW, Zhang T, Liu CY (2007) Oil-gas exploration prospect of dolomite reservoir in the Lower Paleozoic of Tarim Basin. *Acta Petrolei Sin* 28:1–8 (in Chinese with English abstract)
- Zhou ZY (2001) Stratigraphy of the Tarim Basin. Science Press, Beijing, p 359 (in Chinese with English abstract)
- Zhou ZY, Chen PJ, Wang YJ (1990) Biostratigraphy and Geology Evolution in Tarim Basin. Science Press, Beijing, p 399 (in Chinese)
- Zhou LK, Zhou TR, Wang P, Jia RX (1991) Age of Qiulitag Group in NE Tarim Basin. In: Jia RX (ed) *Research of petroleum geology of northern Tarim basin in China: stratigraphy sedimentology*. China University of Geosciences, Wuhan, pp 36–40 (in Chinese)